DESIGN METHODOLOGIES AND PERFORMANCE ANALYSIS OF ENERGY SYSTEMS

Authors
KERİM MARTİN
MELTEM KOŞAN
HİMMET ERDİ TANÜRÜN

BIDGE Publications

DESIGN METHODOLOGIES AND PERFORMANCE ANALYSIS OF ENERGY SYSTEMS

Authors: KERİM MARTİN, MELTEM KOŞAN, HİMMET ERDİ TANÜRÜN

Editor KERİM MARTİN

ISBN: 978-625-372-888-5

1st Edition

Page Layout By: Gozde YUCEL

Publication Date: 20.12.2025

BIDGE Publications

Certificate No: 71374

www.bidgeyayinlari.com.tr - bidgeyayinlari@gmail.com
Krc Bilişim Ticaret ve Organizasyon Ltd. Şti.
Güzeltepe Mahallesi Abidin Daver Sokak Sefer Apartmanı No: 7/9 Çankaya / Ankara

İçindekiler

FOULING IN HEAT EXCHANGERS: MECHANISMS, EFFECTS AND MITIGATION METHODS

Introduction

Heat exchangers are equipment that transfer heat energy from a hot fluid to a cold fluid across a heat transfer surface (Faes et al., 2019). Heat exchangers allow heat transfer between fluids without mixing them and have a wide range of applications: industry, construction, transportation, and other fields (Ding et al., 2024). Many different types of heat exchangers are available, designed to optimize the thermal interaction between fluids, and their classification is given in Figure 1. Two commonly preferred types of heat exchangers are tube and plate heat exchangers (GaneshKumar et al., 2024).

Various forms of heat exchangers are experiencing a high rate of research and application across different sectors. These applications include heating, cooling, and ventilation applications in buildings (Shen et al., 2023), (Cheng et al., 2023), (Radomski et al., 2022), (Zmrhal et al., 2025), thermal energy storage applications (Patel et al., 2025), (Askar et al., 2022) power plants and industrial applications (Duraisamy & Narasimmalu, 2025), (Paśnikowska-Łukaszuk et al., 2022), (Xing et al., 2025) electronic cooling applications (Mokrane & Bourouis, 2024), (Mokrane & Bourouis, 2024). food processing applications (Khan, 2025), (Bianco et al., 2024), (Ghabour & Korzenszky, n.d.) engine cooling and waste heat recovery applications in the automotive and aerospace sectors (Na et al., 2022), (Alkan, 2024), (Zachariae et al., 2023), ((Sciatti et al., 2025), advanced manufacturing applications (Pacheco da Silva et al., 2025), (Ning et al., 2022), (Rao et al., 2025).

Figure 1: Classification of heat exchangers

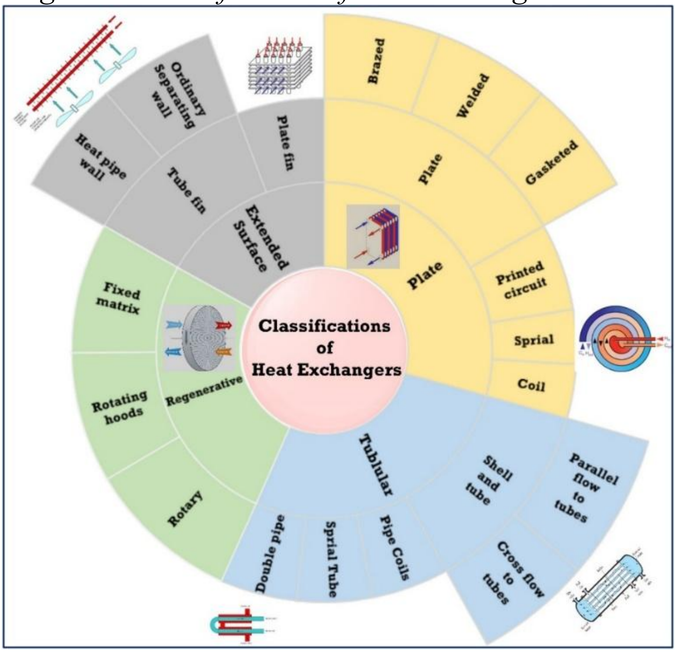

Source:(GaneshKumar et al., 2024)

A review of the current literature reveals that the thermal capacities of heat exchangers vary depending on numerous parameters, and improvement efforts are continuously increasing. Two main methods can be considered for improving the performance of heat exchangers: active and passive methods (Afshari et al., 2021). The active method requires an external energy input, such as an electric field, pulsed flow, or mechanical excitation of the heat transfer surface. The passive method is a heat transfer improvement approach that does not require any external energy support. This method utilizes various applications such as additional structures that increase the surface area, controlled surface roughening techniques, devices that trigger vortex formation in the flow, and flow guides that promote rotational flow (Alam & Kim, 2018). While these methods improve thermal performance, they can also lead to factors such as pressure drop and fouling, which can negatively impact the performance of the heat exchanger(Ahmed et al., 2022).

In heat exchangers, convection or radiation between the fluid and the wall, and conduction along the wall, are effective mechanisms. The magnitude and duration of heat transfer between two fluids depend on the local temperature differences of the fluids and can vary along the heat exchanger (Abd-Elhady & Malayeri, 2016). These transfer mechanisms are significantly affected by fouling of the heat exchanger. Fouling is perhaps the biggest factor causing a decrease in the performance of heat exchangers. A heat exchanger is considered fouled when unwanted substances accumulate on its inner surface, increasing thermal resistance and reducing efficiency (Figure 2). The fouling agent can be an organic or inorganic substance whose thermal conductivity is low compared to the conductivity of the metal wall. Therefore, it causes a decrease in the heat transfer rate (Ben-Mansour et al., 2023). This study reviews the fouling mechanisms and prevention methods of heat exchangers in light of current literature.

Figure 2: Appearance of a clean and a fouled heat exchanger.

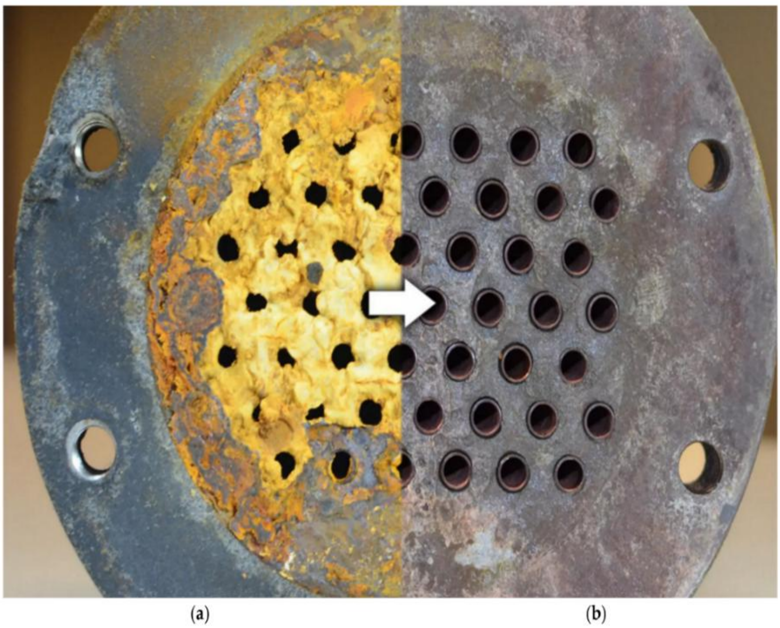

Source: (Ben-Mansour et al., 2023)

The Concept of Fouling in Heat Exchangers

Heat exchangers often involve multiple flow media, and heat transfer occurs between these fluids due to temperature differences. Fluid types vary from application to application, and can cause varying degrees of fouling. This fouling leads to narrowing of the heat exchanger geometry, increased friction, and pressure drop problems. This, in turn, causes the heat exchanger to become unusable in a short time. Among the most common organic foulant are iron oxide, dust and sand in the air, mud and silt in the water, calcium and magnesium salts, while inorganic foulant include carbon, polymers and tars, oils, waxes and greases, bacteria, fungi, and algae (Bott, 1995). Figure 3 shows the interior of a fouled shell-and-tube boiler.

Figure 3: The fouled inner surface of a shell-and-tube boiler

Source: (Bott, 1995)

Fouling in the heat exchanger negatively affects heat transfer mechanisms, leading to a decrease in thermal performance. Since thermal resistance increases on fouled surfaces, heat transfer will be hindered. This phenomenon is schematically shown in Figure 4.

Figure 4: Thermal resistance networks in heat exchangers a) no fouling, b) fouling present

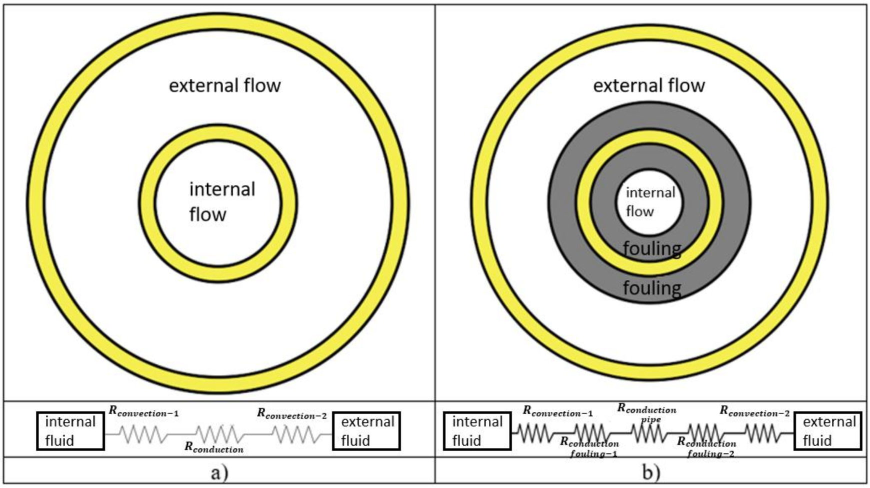

Figure 4 schematically shows the thermal resistance networks in a concentric tube heat exchanger with and without fouling (a) and with fouling (b). In the figure, the thickness of the fouling layer is exaggerated to make the figure clearer. The fouling layer formed on the inner and outer surfaces of the inner tube creates 2 additional thermal resistances. This layer also reduces the heat transfer surface area of the inner tube and negatively affects the heat transfer mechanism. In addition, since the diameter is reduced, the friction force also increases, and a pressure drop problem arises. As mentioned in the previous section, the thermal conductivity of the fouling layers is lower than the thermal conductivity of the tube. Increasing the thickness of the fouling layer negatively affects the heat transfer mechanism and reduces the thermal performance of the heat exchanger. The effect of the resulting thermal resistance networks can be explained by the following equations.

$$\dot{Q} = \frac{\Delta T}{R_{total}} \quad (1)$$

$$R_{total,fouling} = \frac{1}{2h_{in}\pi r_{fouling,in}L} + \frac{ln\frac{r_1}{r_{fouling,in}}}{2\pi k_{fouling}L} + \frac{ln\frac{r_2}{r_1}}{2\pi k_{pipe}L} + \frac{ln\frac{r_{fouling,out}}{r_2}}{2\pi k_{fouling}L} + \frac{1}{2h_{out}\pi r_{fouling,out}L} \quad (2)$$

$$R_{total,clean} = \frac{1}{2h_{in}\pi r_1 L} + \frac{ln\frac{r_2}{r_1}}{2\pi k_{pipe}L} + \frac{1}{2h_{out}\pi r_2 L} \quad (3)$$

In these equations, $\dot{Q}$ represents the total heat transferred from the inner fluid to the outer fluid, R_total represents the total resistance, R_(total,fouled) represents the total resistance when fouling occurs on the inner and outer surfaces of the inner tube, R_(total,clean) represents the total resistance when the tube surfaces are clean, and r_1 and r_2 represent the inner and outer radius of the inner tube, respectively.

Fouling Mechanisms

Contamination mechanisms can be grouped under six different headings:

1. Crystallization fouling or scaling
2. Particle fouling
3. Chemical reaction fouling
4. Corrosion fouling
5. Biological fouling
6. Solidification fouling (Freezing-related fouling)

These mechanisms can occur individually in a heat exchanger, or different types may occur together (Berce et al., 2021). Some images of the fouling caused by these mechanisms in heat exchangers are given in Figure 5.

Figure 5: Images of unfouled and fouled heat exchangers

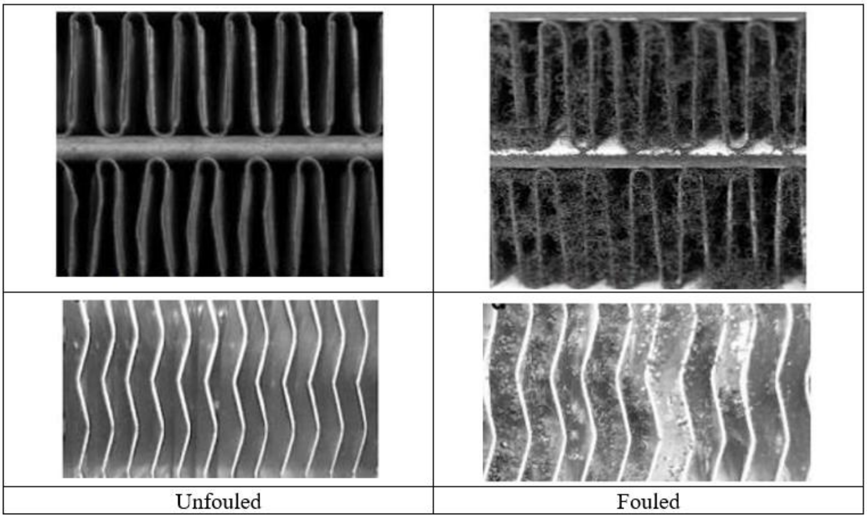

Source: (Sarfraz & Bach, 2016)

The basic fouling process can be divided into different stages such as initiation, transport, accumulation, removal, and aging (Shaikh et al., 2023).

Crystallization fouling or calcification

Essentially, crystallization is the phenomenon of minerals dissolved in a fluid accumulating on the surfaces of heat exchangers. It is a common problem in desalination processes, water heat exchangers, process plants, steam generating units, and household appliances (Shaikh et al., 2023). The increase in the amount of deposition in a heat exchanger varies depending on the ratio of particles accumulating on the surface to particles leaving the surface. If the amount of deposition exceeds the amount of separation, the heat exchanger becomes fouled rapidly. Figure 6 illustrates the principle of these two mechanisms.

Figure 6: Deposition and separation events in the crystallization mechanism

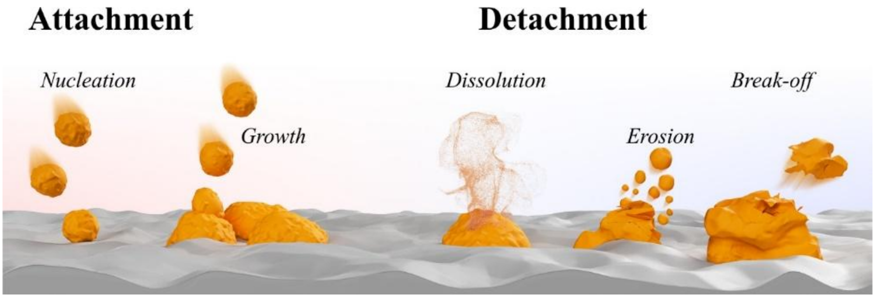

Source: (Løge & Anabaraonye, 2024)

As shown in Figure 7, crystallization fouling, a complex process encompassing several fundamental disciplines, creates numerous problems such as rendering membranes inoperable, restricting access to sanitation and drinking water for approximately 2.6 billion people, reducing heat exchanger efficiency, increasing fuel consumption of marine vessels by up to 60%, causing significant additional costs in underground energy production, and increasing operating costs during freshwater production (Løge & Anabaraonye, 2024).

Figure 7: Crystallization contamination and the key disciplines it affects

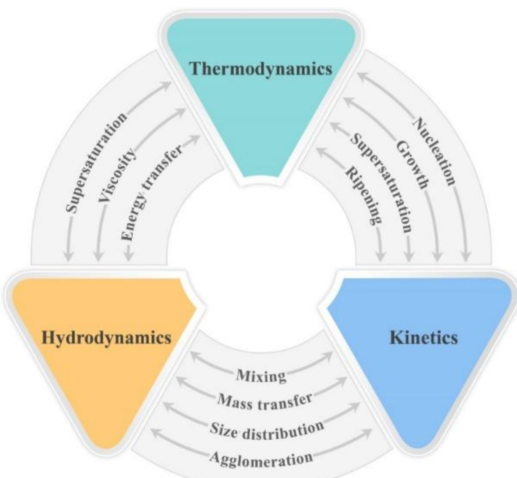

Source: (Løge & Anabaraonye, 2024)

Particle fouling

Particle fouling occurs when floating particles in the process flow begin to accumulate on the heat transfer surface due to transport and deposition. Particle fouling can be divided into two different categories: dry particle deposition and wet particle deposition. Both types of fouling significantly affect the deterioration of heat exchanger performance (Awais & Bhuiyan, 2019). The development of particle fouling is shown in Figure 8 by Abd-Elhady and Malayeri. Here, an asymptotic behaviour is observed, with deposition being excessive initially and decreasing towards the end (Abd-Elhady & Malayeri, 2013).

Figure 8: Development of particle fouling

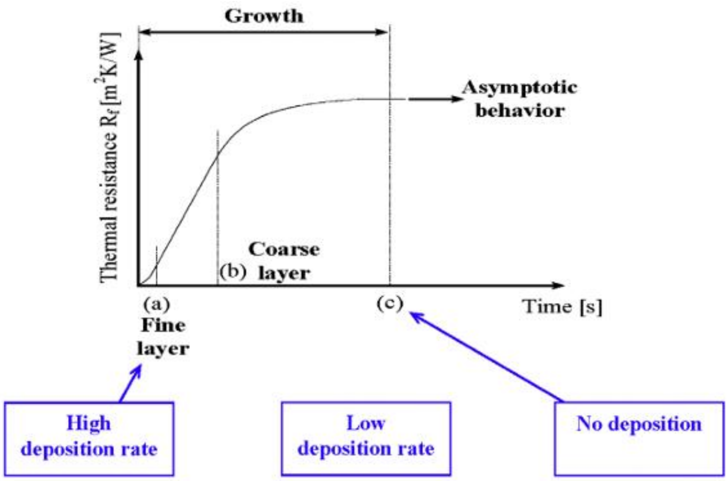

Source: (Abd-Elhady & Malayeri, 2013)

Chemical reaction fouling

Chemical reaction fouling is commonly seen in the food sector, chemical industry, and petroleum processes (Awais & Bhuiyan, 2019). Chemical reaction-related contamination generally consists of a multi-stage process involving interrelated steps, the possible stages of which are shown in Figure 9.

Figure 9: General diagram of the chemical reaction contamination mechanism

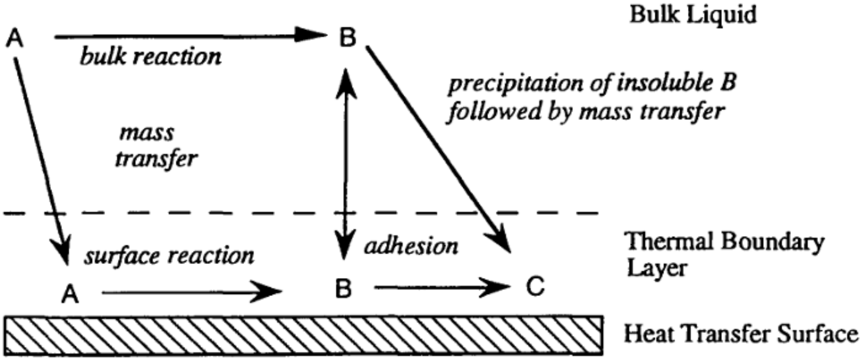

Source: (Watkinson & Wilson, 1997)

In the simplest scenario, precursor compounds that cause fouling enter the heat exchanger along with the fluid and form residues (sediments) as a result of chemical reactions occurring on the wall surface. In another scenario, after substances prone to reactivity enter the heat exchanger, both precursor species and fouling products can form in the fluid, within the thermal boundary layer, or directly on the surface. Therefore, not only the reactions themselves but also the transport of reactants, soluble intermediates, and insoluble pollutants can affect fouling (Watkinson & Wilson, 1997). Reactions that cause organic fluid fouling include polymerization, pyrolysis, and auto-oxidation (Watkinson & Panchal, 1990).

Corrosion fouling

Corrosion is an electrochemical or chemical event that occurs between a material, mostly metallic, and its environment, causing deterioration of the material and its properties. This event refers to the physicochemical relationship between the metal and its surroundings. It causes changes in the properties of the metal. This leads to the functional deterioration of the technical system formed by these two factors (metal and environment) (Alzinkee, 2024). Corrosion fouling in heat exchangers is the fouling caused by electrochemical reactions that can occur between the heat transfer surface and the fluid. Unlike other types of fouling, this fouling event causes permanent damage to heat exchangers (Sarfraz & Bach, 2016). Depending on the pH of the fluid, the residues produced by corrosion can float in the fluid or dissolve and move downstream. In another scenario, corrosion products can accumulate on the surface and negatively affect heat transfer due to their low thermal conductivity coefficients. Liquid-liquid heat exchangers are significantly affected by corrosion fouling (Awais & Bhuiyan, 2019). Corrosion fouling can occur in two different ways. First, corrosion products accumulate and adhere to the surface, creating heat transfer resistance. Second, corrosion products can be transported from the corrosion zone as particulate matter and accumulate as particulate fouling on the heat transfer surface on the other side of the system (Hou, 2018). Figure 10 shows an example of corrosion fouling in a heat exchanger.

Figure 10: A heat exchanger exposed to corrosion contamination

Source: (García & Trueba, 2020)

Biological fouling

Biological fouling can be defined as the accumulation of very small organisms (microorganisms) such as fungi, algae, and bacteria on surfaces. This phenomenon leads to the formation of harmful biofilms, which cause problems in various industrial applications. The first stage of biofilm formation is the rapid adsorption of organic molecules. This organic layer then enhances subsequent microbial adhesion. The next stage is the adhesion of microorganisms to the conditioned surface; this stage is followed by continuous microbial adhesion, enlargement of the adhered cells, and then extracellular polymer production (Al-Ahmad et al., 2000). Figure 11 schematically shows the biofilm formation process in sequence, as created by (Gule et al., 2016).

Figure 11: Stages of biofilm formation (in order)

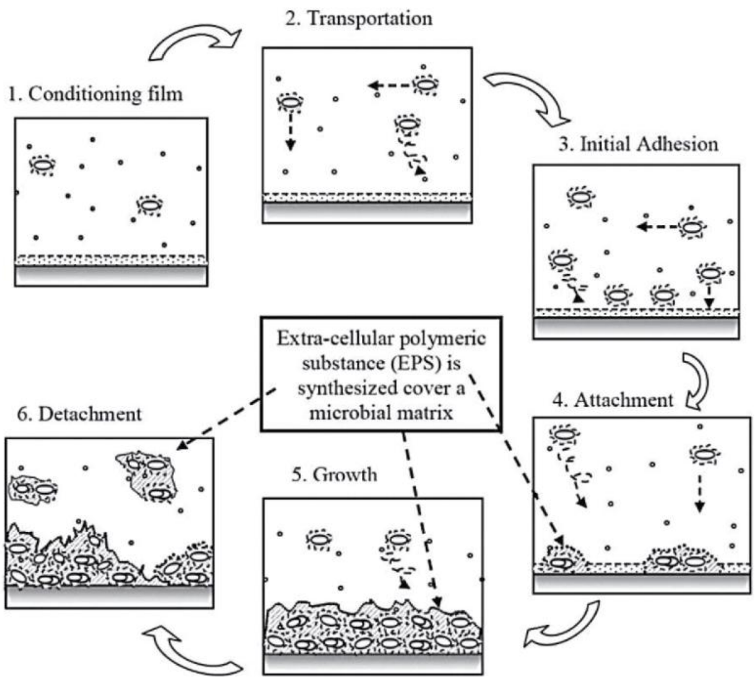

Source: (Gule et al., 2016)

Biological fouling is a common occurrence in numerous applications, including cooling towers and heat exchangers, drinking water and wastewater treatment systems, the food and dairy industry, paper mills, the clinical industry, the agricultural sector, and the petroleum industry (Gule et al., 2016). Additionally, marine or power plant heat exchangers (condensers, boilers) are also highly susceptible to biological fouling (Awais & Bhuiyan, 2019).

Solidification fouling (Freezing-related fouling)

Freeze fouling is the condition in which a colder environment than the average temperature of the fluid is formed in the heat transfer area due to the solidification of the solvent itself or dissolved substances. Therefore, it is considered a special case of crystallization fouling. A schematic representation of freeze-induced fouling is shown in Figure 12. However, the formation of frozen parts from the flowing fluid is not only a concern in heat exchanger fouling; the accumulation of wax fractions, narrowing the channel diameter and causing pressure drop in underwater oil pipelines, is also a frequently encountered problem (Fernandez-Torres et al., 2001).

Figure 12: Schematic representation of freeze fouling

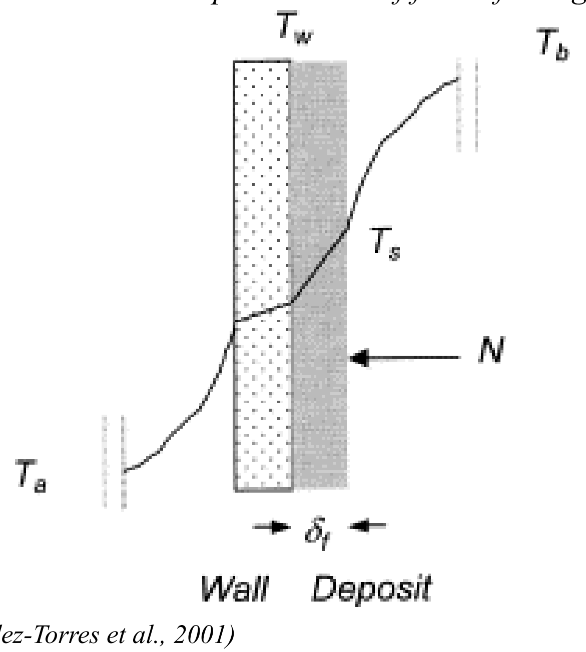

Source: (Fernandez-Torres et al., 2001)

Frost (solidification) fouling causes deposits to accumulate on the heat transfer surface area, creating additional resistance and negatively affecting the thermal performance of the heat exchanger. It also causes a reduction in diameter for circular cross-sections and consequently a pressure drop problem.

The Effects of Fouling on Heat Transfer

Studies show that fouling in heat exchangers has significant negative effects on the efficiency and performance of heat transfer devices. These include economics, productivity, and energy consumption. Due to rising fuel costs, resource depletion, and concerns about environmental impact, energy efficiency has become a dominant factor in most food processing, chemical, and energy production stages (Ogbonnaya & Ajayi, 2017).

Another researcher argued that the accumulation of fouling on heat transfer surfaces negatively affects the performance of the heat exchanger and increases the associated energy consumption (Demirskiy et al., 2018). In another study on fouling in heat exchangers, Xu et al. experimentally investigated the fouling properties of sodium carboxymethyl cellulose inhibitor on the heat transfer surface of $CaCO_3$. In the experiments, the researchers considered sodium carboxymethyl cellulose concentration, solution inlet temperature, mass flow rate, sodium carboxymethyl cellulose substitution degree, and sodium carboxymethyl cellulose viscosity as variables and examined the effects of these variables on fouling inhibition. The results showed that the thermal resistance of fouling decreased with increasing sodium carboxymethyl cellulose concentration. Furthermore, Xu et al. observed that lowering the solution temperature also decreased the thermal resistance of fouling, but increasing the mass flow rate increased the thermal resistance. In addition, it was emphasized that the effect of sodium carboxymethyl cellulose viscosity on the thermal resistance to contamination is negligible (Z. Xu et al., 2021).

Heat exchangers are heat transfer equipment used in many sectors, and their contamination causes significant performance degradation. One of these sectors is dairy processing plants. Highlighting that fouling is a significant cost factor in the dairy industry, frequently leading to plant shutdowns and increased energy demand, Pelz et al. investigated the fouling behaviour of whey protein concentrate. They used polyether ether ketone and talcum powder as heat exchangers and compared the results to a reference stainless steel. Their findings showed that both polymers were able to maintain heat transfer under fouling conditions that steel could not. It was emphasized that the use of polymers resulted in up to a 40% reduction in heat resistance, making these materials an economically viable option for processes with high whey protein concentrations or high heat flow. When comparing the two polymers they used, the researchers did not find a significant difference between them. Higher roughness of talcum powder also had no effect on fouling, and therefore Pelz et al. evaluated talcum powder as the most promising alternative to the reference stainless steel (Philipp Pelz et al., 2024). Another sector where heat exchangers are used extensively is the crude oil processing sector. In these processes, fouling in the heat exchanger will significantly affect the economic efficiency of the process. In a study on this subject, Emani et al. investigated the effects of operation parameters on fouling using CFD. In the study, a three-dimensional CFD model of the heat exchanger tube was developed to predict the coke deposition rate and fouling resistance. The coke deposition rate and fouling resistance were predicted by varying the flow rate, wall shear stress, and surface roughness. Researchers observed that resistance to fouling decreased under conditions of wall shear stress and surface roughness, respectively, compared to non-slip and smooth surfaces (Emani et al., 2017).

Methods for Preventing and Mitigating Pollution

Preventing fouling and particle accumulation in heat exchangers is a crucial and indispensable issue in all areas of industry. Fouling is one of the main reasons that can negatively affect the thermal performance of heat exchangers and create back pressure requiring a large amount of pumping power. Therefore, proper cleaning is recommended to ensure the smooth operation of heat exchangers. The cleaning of heat exchangers can be categorized into two types: online (chemical, mechanical, and physical mechanisms) and offline (Awais & Bhuiyan, 2019).

Online cleaning refers to maintaining heat transfer surfaces at a reasonable cleanliness level to preserve high operational efficiency and plant availability. Online cleaning consists of different methodologies that can be classified, in order of applicability, as:

1. Modifying operating conditions,
2. Chemical
3. Mechanical
4. Physical

approaches (Müller-Steinhagen et al., 2011).

Even if the heat exchanger is well-designed and the fluid treatment process is effective, it will still require periodic cleaning. It is advantageous to remove non-protective deposits as soon as their formation begins (Müller-Steinhagen et al., 2011). Figure 13 shows online and offline methods.

Figure 13: Online and offline cleaning methods

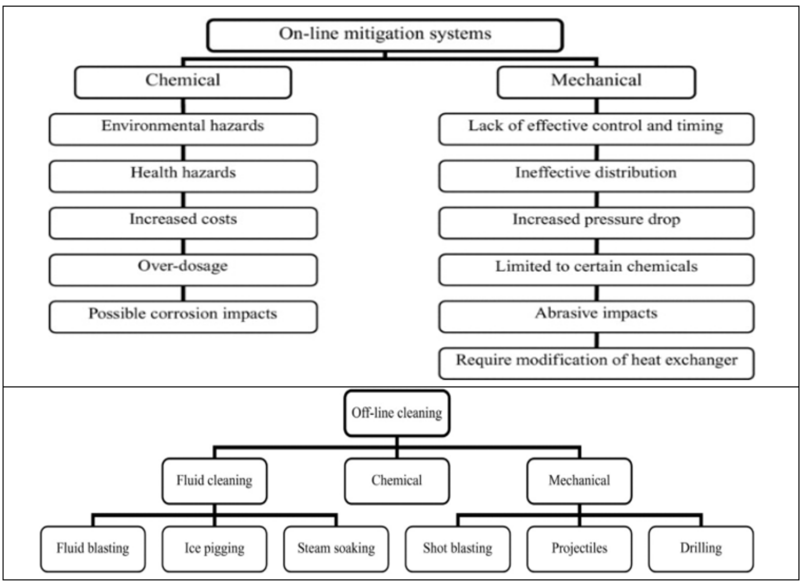

Source: (Müller-Steinhagen et al., 2011)

The choice of one or more of these methods largely depends on the type and material of the heat exchanger, the severity of fouling, the fouling mechanisms, the operating conditions, the resulting costs, and the desired results (Berce et al., 2021).

Teng et al. conducted research on reducing calcium sulfate scaling in a heat exchanger using physical water treatment (PWT) with zinc and tourmaline catalytic materials. The researchers performed a series of experiments with the hypothesis that catalytic materials like zinc and tourmaline could solve fouling problems. Their results showed a reduction in calcium sulfate formation in experiments with high PWT (Figure 14). However, Teng et al. also observed that the performance of PWT gradually decreased over time and emphasized that this issue also needs to be addressed (Teng et al., 2016).

Figure 14: Calcium accumulation

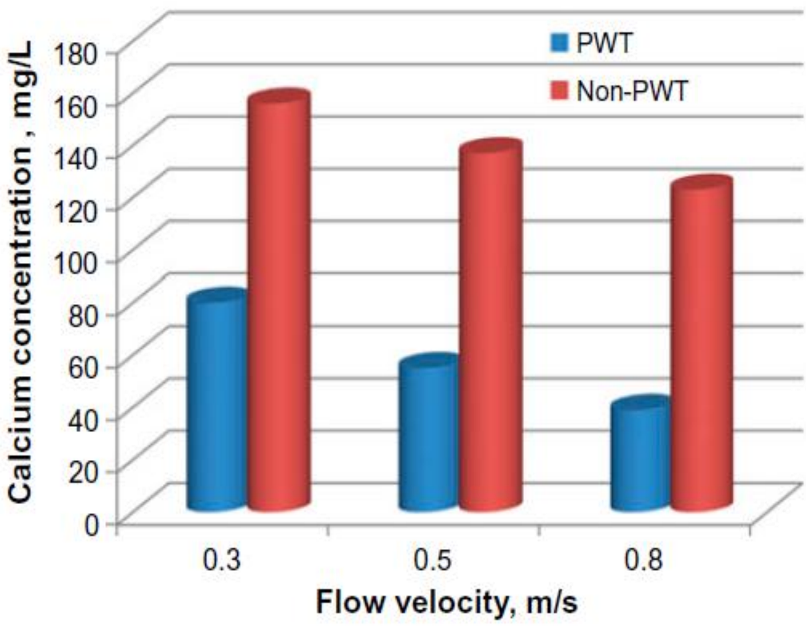

Source: (Teng et al., 2016)

In their experimental study, Kazi et al. investigated the performance of three different types of fibers, added at varying concentrations to a supersaturated mineral salt of calcium sulfate, in delaying fouling in a heat exchanger. Their results showed that physical properties of the fibers, such as density, elasticity, and length, were effective in reducing fouling. The researchers also concluded that reducing fiber length and elasticity at the same concentration would increase the delay in fouling (Kazi et al., 2013).

Shin et al. argued that eddy flows reduce fouling but that this flow cannot be achieved in compact heat exchangers, and proposed a 3D-designed heat exchanger that generated eddy flows better than the classic 2D heat exchanger. They observed that the proposed 3D channels exhibited comparable thermal-hydraulic performance to conventional 2D heat exchanger channels, in addition to their potential to reduce fouling (Shin et al., 2024).

Sarafraz et al. conducted a study to investigate the effects of low-frequency vibration on the fouling behaviour of a chevron-type plate heat exchanger using nanofluids. They applied low-frequency vibration to reduce nanoparticle fouling inside the heat exchanger and compared the results. The researchers' findings showed that nanoparticle fouling can be reduced through low-frequency vibration, and that the thermal resistance of the fouling decreases with the application of vibration to the system. As shown in Figure 15, the application of vibration to the heat exchanger prevented the accumulation of nitrogen bubbles. Furthermore, they observed that continuous vibration of the heat exchanger improved the overall thermal performance of the system, while in the absence of vibration, continuous particle fouling occurred on the inner wall of the heat exchanger, thus increasing the thermal resistance (Sarafraz et al., 2017). Vemireddi and Palte also conducted a study on low-frequency application and showed that they achieved a significant increase in heat transfer in the presence of ultrasonic vibration (Vemireddi & Patle, 2025).

Figure 15: Appearance of fouling conditions obtained by Sarafraz et al. in non-vibrating and vibrating states

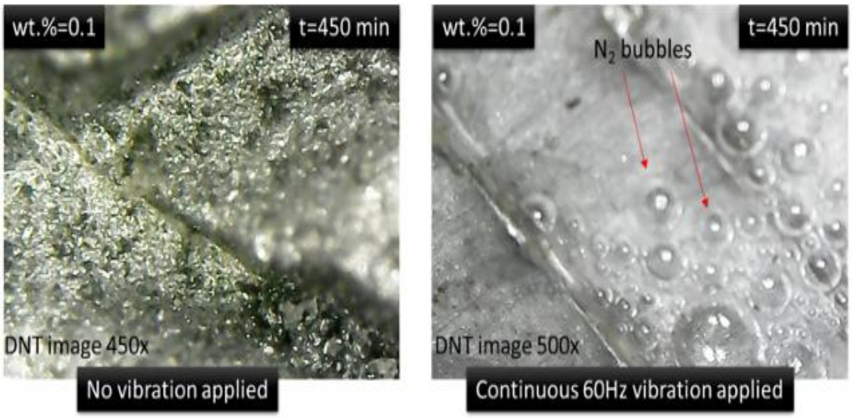

Source: (Sarafraz et al., 2017)

Schnöing and colleagues argued that surface modifications in heat exchangers, particularly those used in the food industry, could reduce the effects of fouling, and conducted a literature review examining approximately 100 studies in this context. Based on the studies they reviewed, they concluded that surface modifications of heat exchangers would reduce fouling (Schnöing et al., 2020).

The use of surfactants can be effective in reducing fouling in heat exchangers. Hasan et al. conducted a study on this topic, using alkylbenzene sulfonate as a surfactant. Their research revealed that decreasing fluid temperature increased the thermal resistance to fouling. They also observed that a higher dispersed oil fraction resulted in higher thermal resistance at all temperatures due to higher oil accumulation. The researchers found that adding alkylbenzene sulfonate at a volumetric ratio of 0.2% to 0.5% significantly reduced thermal resistance, depending on the oil fraction and Reynolds number (Figure 16). They also observed that the percentage reduction was higher for lower Reynolds numbers, reaching up to 96% (Hasan et al., 2020).

Figure 16: Effect of surfactant on thermal resistance

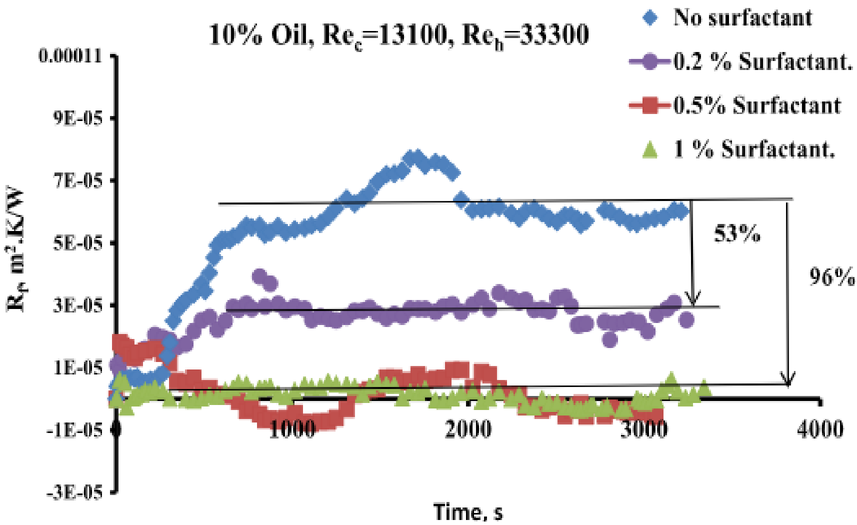

Source: (Hasan et al., 2020)

Radiators used in building heating systems are also heat exchangers. Cleaning them at certain intervals reduces the thermal resistance caused by contamination, thus improving thermal performance. In a study conducted by Yürük et al. in 2022, radiators in a residence using an individual heating system were cleaned using certain chemicals, and it was observed that the heat distribution in the radiators was more even, thus increasing thermal performance. The researchers supported the results they obtained in the study with a thermal camera image presented in Figure 17. Figure 17 shows that the heat distribution improved because of removing the contamination (Yürük et al., 2022).

Figure 17: Thermal camera image showing the effect of radiator cleaning on heat distribution

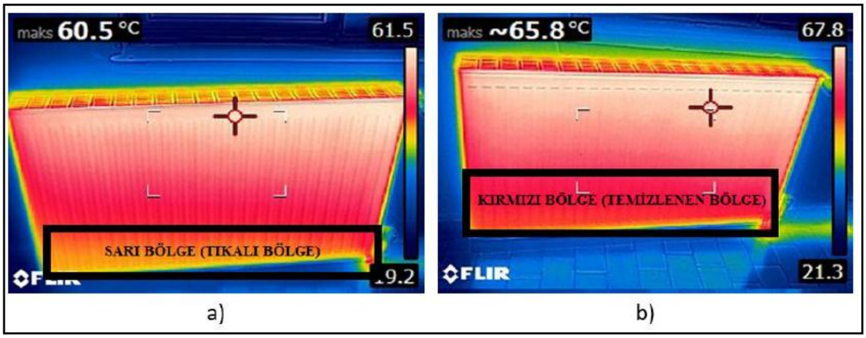

Source: (Yürük et al., 2022)

Conclusion

Heat exchangers are one of the pieces of equipment that provide efficient heat transfer in industry and many other sectors. The performance of heat exchangers is controlled by numerous parameters, and efforts to improve their performance are constantly underway. On the other hand, fouling is a parameter that negatively affects the performance of heat exchangers and is always a subject that researchers focus on. Fouling in heat exchangers is not only an event that reduces heat transfer performance; it is also a process that has significant consequences in terms of operational reliability and energy efficiency. When studies in the literature are examined, it is seen that fouling occurs through multiple mechanisms. In particular, particulate fouling, crystallization, biological fouling, and corrosion fouling can develop simultaneously or trigger each other in many applications.

The most significant effect of fouling is that it creates additional thermal resistance on the heat transfer surface, leading to a decrease in the overall heat transfer coefficient. In addition, increased pressure losses due to narrowing of the flow cross-section cause the system to operate with higher energy consumption. In long-term operation, especially in cases of corrosion-related fouling, risks of material loss, surface damage, and leakage can arise; this shortens the economic life of the heat exchanger. Therefore, fouling in heat exchangers is a problem that needs to be addressed not only in terms of thermal performance but also in terms of maintenance and continuity.

Some studies in the literature have emphasized that the fouling problem can be reduced through design measures before reaching the cleaning stage. When evaluating methods for preventing fouling, different strategies stand out depending on the application. Research frequently mentions two main strategies: online and offline methods.

Recent studies show that online measurement techniques, numerical models, and predictive maintenance approaches have gained importance for monitoring and controlling fouling. These approaches allow for the early identification of fouling trends and the development of appropriate intervention strategies. However, long-term field data and standardized evaluation criteria are needed for these methods to become widespread in industrial applications.

Generally, effective management of fouling in heat exchangers is possible through a correct understanding of the mechanisms, the selection of prevention methods appropriate to the system's operating conditions, and the implementation of regular monitoring strategies. In this context, fouling control should be considered an integral part of modern heat exchanger design and operation.

References

Abd-Elhady, M. S., & Malayeri, M. R. (2013). Asymptotic characteristics of particulate deposit formation in exhaust gas recirculation (EGR) coolers. *Applied Thermal Engineering*, *60*(1–2), 96–104. https://doi.org/10.1016/j.applthermaleng.2013.06.038

Abd-Elhady, M. S., & Malayeri, M. R. (2016). Transition of convective heat transfer to subcooled flow boiling due to crystallization fouling. *Applied Thermal Engineering*, *92*, 122–129. https://doi.org/10.1016/j.applthermaleng.2015.09.093

Afshari, F., Sözen, A., Khanlari, A., & Tuncer, A. D. (2021). Heat transfer enhancement of finned shell and tube heat exchanger using Fe2O3/water nanofluid. *Journal of Central South University*, *28*(11), 3297–3309. https://doi.org/10.1007/s11771-021-4856-x

Ahmed, R., Babat, A., Sözen, A., Martin, K., Aytaç Yilmaz, Z., Halil, &, & Variyenli, İ. (2022). Improvıng The Thermal Performance Of Concentrıc-Tube Heat Exchangers Usıng Magnetıc Nanofluıds. *Heat Transfer Research*, *53*(15), 17–38. www.begellhouse.com

Al-Ahmad, M., Aleem, F. A. A., Mutiri, A., & Ubaisy, A. (2000). Biofuoling in RO membrane systems Part 1: Fundamentals and control. *Desalination*, *132*, 173–179. www.elsevier.com/locate/desal

Alam, T., & Kim, M. H. (2018). A comprehensive review on single phase heat transfer enhancement techniques in heat exchanger applications. *Renewable and Sustainable Energy Reviews*, *81*(August 2017), 813–839. https://doi.org/10.1016/j.rser.2017.08.060

Alkan, A. (2024). Experimental study on the impact of indoor unit airflow velocity on the performance of an automotive heat pump system with a suction line heat exchanger. *Heliyon*, *10*(17). https://doi.org/10.1016/j.heliyon.2024.e36719

Alzinkee, A. A. (2024). A Study Of Corrosion In Oil And Gas Tanks. *Frontiers in Health Informatics*, *13*(3), 10322–10340. www.healthinformaticsjournal.com

Askar, S., Fotowat, S., Momeni, M., & Fartaj, A. (2022). Transient experimental study of a latent heat thermal energy storage in a heat exchanger for effective thermal management. *Journal of Energy Storage*, *55*. https://doi.org/10.1016/j.est.2022.105680

Awais, M., & Bhuiyan, A. A. (2019). Recent advancements in impedance of fouling resistance and particulate depositions in heat exchangers. In *International Journal of Heat and Mass Transfer* (Vol. 141, pp. 580–603). Elsevier Ltd. https://doi.org/10.1016/j.ijheatmasstransfer.2019.07.011

Ben-Mansour, R., El-Ferik, S., Al-Naser, M., Qureshi, B. A., Eltoum, M. A. M., Abuelyamen, A., Al-Sunni, F., & Ben Mansour, R. (2023). Experimental/Numerical Investigation and Prediction of Fouling in Multiphase Flow Heat Exchangers: A Review. In *Energies* (Vol. 16, Issue 6). MDPI. https://doi.org/10.3390/en16062812

Berce, J., Zupančič, M., Može, M., & Golobič, I. (2021). A review of crystallization fouling in heat exchangers. In *Processes* (Vol. 9, Issue 8). MDPI AG. https://doi.org/10.3390/pr9081356

Bianco, V., Cascetta, F., & Nardini, S. (2024). Application of nanofluids in industrial processes. The case of food processing. *Thermal Science and Engineering Progress*, *53*. https://doi.org/10.1016/j.tsep.2024.102726

Bott, T. , R. (1995). *Fouling of Heat Exchangers*. Elsevier.

Cheng, N., Zhou, C., Luo, Y., Shen, J., Tian, Z., Sun, D., Fan, J., Zhang, L., Deng, J., & Rosen, M. A. (2023). Thermal behavior and performance of shallow-deep-mixed borehole heat exchanger array for sustainable building cooling and heating. *Energy and Buildings*, *291*. https://doi.org/10.1016/j.enbuild.2023.113108

Demirskiy, O. V., Kapustenko, P. O., Arsenyeva, O. P., Matsegora, O. I., & Pugach, Y. A. (2018). Prediction of fouling tendency in PHE by data of on-site monitoring. Case study at sugar factory. *Applied Thermal Engineering*, *128*, 1074–1081. https://doi.org/10.1016/j.applthermaleng.2017.09.087

Ding, Y., Guo, Q., Guo, W., Chu, W., & Wang, Q. (2024). Review of Recent Applications of Heat Pipe Heat Exchanger Use for Waste Heat Recovery. In *Energies* (Vol. 17, Issue 11). Multidisciplinary Digital Publishing Institute (MDPI). https://doi.org/10.3390/en17112504

Duraisamy, K., & Narasimmalu, R. (2025). Optimizing Heat Exchanger Performance and Thermal Efficiency Using Different Fluid Blends in Power Plants. *Heat Transfer*. https://doi.org/10.1002/htj.70067

Emani, S., Yusoh, N. A., Gounder, R. M., & Shaari, K. Z. K. (2017). Effect of operating conditions on crude oil fouling through CFD simulations. *International Journal of Heat and Technology*, *35*(4), 1034–1044. https://doi.org/10.18280/ijht.350440

Faes, W., Lecompte, S., Ahmed, Z. Y., Van Bael, J., Salenbien, R., Verbeken, K., & De Paepe, M. (2019). Corrosion and corrosion prevention in heat exchangers. In *Corrosion Reviews* (Vol. 37, Issue 2, pp. 131–155). De Gruyter. https://doi.org/10.1515/corrrev-2018-0054

Fernandez-Torres, M. J., Fitzgerald, A. M., Paterson, W. R., & Wilson, D. I. (2001). A theoretical study of freezing fouling: limiting behaviour based on a heat and mass transfer analysis. In *Chemical Engineering and Processing* (Vol. 40). www.elsevier.com/locate/cep

GaneshKumar, P., VinothKumar, S., Vigneswaran, V. S., Kim, S. C., & Ramkumar, V. (2024). Advancing heat exchangers for energy storage: A comprehensive review of methods and techniques. In *Journal of Energy Storage* (Vol. 99). Elsevier Ltd. https://doi.org/10.1016/j.est.2024.113334

García, S., & Trueba, A. (2020). Fouling in Heat Exchangers. In *Inverse Heat Conduction and Heat Exchangers*. Natl Res Counc of Can. https://doi.org/doi:10.5772/intechopen.80096.

Ghabour, R., & Korzenszky, P. (n.d.). Dynamic Modelling and Experimental Analysis of Tankless Solar Heat Process System for Preheating Water in the Food Industry. In *Acta Polytechnica Hungarica* (Vol. 20, Issue 4).

Gule, N. P., Begum, N. M., & Klumperman, B. (2016). Advances in biofouling mitigation: A review. *Critical Reviews in Environmental Science and Technology*, *46*(6), 535–555. https://doi.org/10.1080/10643389.2015.1114444

Hasan, B. O., Hathal, M. M., & Sh Majdi, H. (2020). Study on oil fouling in a double pipe heat exchanger with mitigation by a surfactant. *Heat Transfer - Asian Research*, *49*(5), 2645–2658. https://doi.org/10.1002/htj.21738

Hou, T. K. (2018). *Foulıng And Its Mıtıgatıon On Heat Exchanger Surfaces By Addıtıves And Catalytıc Materıals* [Doctoral thesis]. University of Malaya.

Kazi, S. N., Duffy, G. G., & Chen, X. D. (2013). Fouling mitigation of heat exchangers with natural fibres. *Applied Thermal Engineering*, *50*(1), 1142–1148. https://doi.org/10.1016/j.applthermaleng.2012.08.042

Khan, M. S. (2025). Computational heat transfer analysis of liquid food in a heat exchanger with varying stirrer settings in a nonclassical continuum framework. *Numerical Heat Transfer, Part B: Fundamentals*, *86*(4), 1138–1157. https://doi.org/10.1080/10407790.2024.2302859

Løge, I. A., & Anabaraonye, B. U. (2024). The importance of detachment processes in modeling crystallization fouling. In *Chemical Engineering Journal* (Vol. 497). Elsevier B.V. https://doi.org/10.1016/j.cej.2024.154642

Mokrane, M., & Bourouis, M. (2024). Heat Transfer and Fluid Flow Characteristics in a Micro Heat Exchanger Employing Warm Nanofluids for Cooling of Electronic Components. *Energies* , *17*(10). https://doi.org/10.3390/en17102383

Müller-Steinhagen, H., Malayeri, M. R., & Watkinson, A. P. (2011). Heat exchanger fouling: Mitigation and cleaning strategies. *Heat Transfer Engineering*, *32*(3–4), 189–196. https://doi.org/10.1080/01457632.2010.503108

Na, S. I., Kim, M., & Kim, M. S. (2022). Performance analysis of an automotive heat pump system with desiccant coated heat exchangers. *Applied Thermal Engineering*, *213*. https://doi.org/10.1016/j.applthermaleng.2022.118723

Ning, J., Wang, X., Sun, Y., Zheng, C., Zhang, S., Zhao, X., Liu, C., & Yan, W. (2022). Experimental and numerical investigation of additively manufactured novel compact plate-fin heat exchanger. *International Journal of Heat and Mass Transfer*, *190*. https://doi.org/10.1016/j.ijheatmasstransfer.2022.122818

Ogbonnaya, S. K., & Ajayi, O. O. (2017). Fouling phenomenon and its effect on heat exchanger: A review. *Frontiers in Heat and Mass Transfer*, *9*. https://doi.org/10.5098/hmt.9.31

Pacheco da Silva, R. P., Muneeshwaran, M., Krishnan, E. N., Li, X., Nawaz, K., & Kim, H. J. (2025). Advances in high-pressure and high-temperature heat exchangers: Innovations via additive manufacturing and their applications. In *Thermal Science and Engineering Progress* (Vol. 65). Elsevier Ltd. https://doi.org/10.1016/j.tsep.2025.103844

Paśnikowska-Łukaszuk, M., Wójcicka-Migasiuk, D., & Wośko, E. (2022). Daily Analysis of Changes Taking Place in Heat Exchangers Used in Combined Heat and Power Plants. *Advances in Science and Technology Research Journal*, *16*(6), 258–266. https://doi.org/10.12913/22998624/156492

Patel, M., Chaudhary, V., Verma, V., Kumar, A., & Kakati, B. K. (2025). Advances in ground heat exchangers and thermal energy storage for sustainable energy systems. *Indian Chemical Engineer*, *67*(4), 429–449. https://doi.org/10.1080/00194506.2025.2454246

Philipp Pelz, Jonas Noß, Erik von Harbou, & Hans-Jörg Bart. (2024). Whey protein fouling on polymeric heatexchangers. *Heat Transfer*, *53*(6), 2948–2964.

Radomski, B., Kowalski, F., & Mróz, T. (2022). The Direct-Contact Gravel, Ground, Air Heat Exchanger—Application in Single-Family Residential Passive Buildings †. *Energies*, *15*(17). https://doi.org/10.3390/en15176110

Rao, Y., Zhang, Y., & Xiao, K. (2025). Experimental and numerical study of thermal performance of an additively manufactured microchannel heat exchanger. *Thermal Science and Engineering Progress*, *62*. https://doi.org/10.1016/j.tsep.2025.103572

Sarafraz, M. M., Nikkhah, V., Madani, S. A., Jafarian, M., & Hormozi, F. (2017). Low-frequency vibration for fouling mitigation and intensification of thermal performance of a plate heat exchanger working with CuO/water nanofluid. *Applied Thermal Engineering*, *121*, 388–399. https://doi.org/10.1016/j.applthermaleng.2017.04.083

Sarfraz, O., & Bach, C. K. (2016). *A Literature Review on Air Side Heat Exchanger Fouling in Heating, Ventilation and Air-Conditioning (HVAC) Applications*. http://docs.lib.purdue.edu/iracc/1663

Schnöing, L., Augustin, W., & Scholl, S. (2020). Fouling mitigation in food processes by modification of heat transfer surfaces: A review. In *Food and Bioproducts Processing* (Vol. 121, pp. 1–19). Institution of Chemical Engineers. https://doi.org/10.1016/j.fbp.2020.01.013

Sciatti, F., Di Domenico, V., Tamburrano, P., Distaso, E., & Amirante, R. (2025). An Innovative Cryogenic Heat Exchanger Design for Sustainable Aviation. *Energies*, *18*(5). https://doi.org/10.3390/en18051261

Shaikh, K., Newaz, K. M. S., Zubir, M. N. M., Wong, K. H., Khan, W. A., Abdullah, S., Alam, M. S., & Sugumaran, L. (2023). A review of recent advancements in the crystallization fouling of heat exchangers. In *Journal of Thermal Analysis and Calorimetry* (Vol. 148, Issue 22, pp. 12369–12392). Springer Science and Business Media B.V. https://doi.org/10.1007/s10973-023-12544-z

Shen, C., Zhang, B., Zhang, D., Zhang, Y., Wei, S., & Yang, S. (2023). Experimental study on the parallel-flow heat pipe heat exchanger for energy saving in air conditioning. *Journal of Building Engineering*, *75*. https://doi.org/10.1016/j.jobe.2023.106842

Shin, S. M., Lee, S. W., Chung, S., Kim, N., Kim, M. H., & Jo, H. J. (2024). Mitigation of fouling with swirling flow induced in 3-D double-sided straight channel for printed circuit heat exchanger. *International Journal of Heat and Mass Transfer*, *233*. https://doi.org/10.1016/j.ijheatmasstransfer.2024.125982

Teng, K. H., Baharudin, R. H., Bakar, M. A., & Kazi, S. N. (2016). Mitigation of heat exchanger fouling in industry using catalytic materials. *Desalination and Water Treatment*, *57*(1), 22–27. https://doi.org/10.1080/19443994.2015.1012334

Vemireddi, S., & Patle, S. Das. (2025). Experimental investigation on the fouling mitigation and enhancement of heat transfer in a double-pipe heat exchanger in the presence of low-frequency vibrations. *World Journal of Engineering*, *Early Access*.

Watkinson, A. P., & Panchal, C. B. (1990, July). *A Crıtıcal Revıew of Organıc Fluıd Foulıng*.

Watkinson, A. P., & Wilson, D. I. (1997). Chemical Reaction Fouling: A Review. *Experimental Thermal and Fluid Science*, *14*, 361–374.

Xing, T., Jiang, M., Zhu, X., Han, B., Xu, J., Yang, X., & Ji, M. (2025). Recursive data reconciliation with nonlinear characteristic constraints for typical heat exchangers in nuclear power plant. *Annals of Nuclear Energy*, *212*. https://doi.org/10.1016/j.anucene.2024.111054

Xu, Z., Zhao, Y., He, J., Qu, H., Wang, Y., & Wang, B. (2021). Fouling characterization of calcium carbonate on heat transfer surfaces with sodium carboxymethyl cellulose as an inhibitor. *International Journal of Thermal Sciences*, *162*. https://doi.org/10.1016/j.ijthermalsci.2020.106790

Yürük, M., Variyenli, H., Martin, K., Khanları, A., & Aytaç, İ. (2022). Bireysel Isıtma Sistemlerinde Tesisat Temizliğinin Enerji Verimliliği Açısından Deneysel Olarak Değerlendirilmesi. *Politeknik Dergisi*, *25*(3), 1375–1384. https://doi.org/10.2339/politeknik.1025494

Zachariae, J., Tiesler, M., Singh, R., Benning, T. A., & Schweikert, C. (2023). Silicon carbide based traction inverter cooling in electric vehicle using heat pipes. *Thermal Science and Engineering Progress*, *46*. https://doi.org/10.1016/j.tsep.2023.102155

Zmrhal, V., Kubenthiran, J., & Zelenský, P. (2025). Sensible heat effectiveness of rotary heat exchangers at low rotational speeds. *Energy and Buildings*, *342*. https://doi.org/10.1016/j.enbuild.2025.115905

PHOTOVOLTAIC PANELS AND THE EFFECT OF ENVIRONMENTAL CONDITIONS ON THEIR PERFORMANCE

Introduction

The global energy landscape is undergoing a dramatic transition driven by two urgent challenges: climate change and the increasing demand for sustainable, secure energy sources. Conventional fossil fuels (coal, oil, and natural gas) are finite resources whose combustion releases massive amounts of greenhouse gases, primarily carbon dioxide (CO_2), which is the leading cause of global warming. In this context, solar energy emerges as the single most critical and abundant solution (Skoplaki & Palyvos, 2009). The sun is the largest power source available to humanity, radiating of energy to the Earth continuously an amount thousands of times greater than the world's current energy consumption. Harnessing even a small fraction of this energy can meet global power needs sustainably. Furthermore, solar energy offers energy independence and reduces geopolitical risks associated with relying on localized fossil fuel supplies (Notton & et al., 2005).

Photovoltaics (PV) is the direct conversion of light into electricity at the atomic level, achieved through the photovoltaic effect. The term is derived from the Greek word phōs (light) and volt, named after Alessandro Volta, a pioneer in electricity. At the core of PV technology is the solar cell, which acts as a solid-state electronic device. These cells are typically made from semiconductor materials, most commonly silicon. When sunlight (composed of particles called photons) strikes the cell, the PV effect causes the photons to knock electrons loose from their atoms. A built-in electric field then forces these free electrons to flow in a specific direction, creating a Direct Current (DC) electricity (Parida, Iniyan, & Goic, 2011).

A single solar cell produces only a small amount of power (typically under 1 Watt). To generate usable electricity, multiple solar cells are electrically connected in series and parallel, sealed within a protective frame (usually glass and aluminum) for environmental durability, and assembled into a functional unit called a photovoltaic module, more commonly known as a solar panel.These panels form the foundation of PV systems, which can range in size from small calculators to massive utility-scale power plants, collectively making PV a cornerstone of the modern renewable energy infrastructure.

PV panels are a cornerstone of the sustainable energy quest due to their environmental friendliness and access to an unlimited supply. However, the real-time performance of a PV system is determined not by how cleanly it is produced, but by the complex interaction of the environmental conditions to which the panels are constantly exposed. Because panels operate outside of standard laboratory test conditions (25°C and 1000 W/m^2), performance evaluation must always be adjusted for environmental influences (Arslan & et al., 2023).

The primary environmental factors affecting panel efficiency include solar radiation intensity, temperature, and physical obstructions. Irradiance, the primary determinant of the electrical current drawn from a panel, is directly reduced by factors such as cloud cover, fog, or atmospheric pollution. Conversely, temperature is the factor that most significantly reduces cell efficiency; as panel temperature rises above 25°C, the cell voltage, and therefore the total power output, decreases. Furthermore, shading caused by physical obstructions such as trees, chimneys, or snow, can cause disproportionate and significant losses in series-connected cells, causing the shaded cell to limit the performance of the entire panel (Aktaş & et al., 2024). Therefore, PV system design and layout should be optimized to minimize environmental losses, taking into account local climate and geographical characteristics.

PV technology represents a cornerstone of the renewable energy revolution, offering a clean, sustainable, and reliable method of power generation by utilizing the sun's abundant energy. The key takeaways of photovoltaic panels can be summarized as: Solar energy is vital for mitigating climate change and achieving long-term energy sustainability. The sun provides energy far exceeding global demands. PV technology converts light directly into electricity using the photovoltaic effect in semiconductor materials. The fundamental unit is the solar cell, which is combined to form the solar panel.

The Physics Behind the Photovoltaic Effect

The conversion of sunlight into electrical energy is achieved through the photovoltaic effect, a phenomenon rooted in solid-state physics. The photovoltaic effect, in its simplest form, is the process of directly converting light energy (photons) into electrical energy. This is typically achieved using semiconductor materials (Hernández-Callejo, Gallardo-Saavedra, & Alonso-Gómez, 2019).

Photons and energy light is composed of energy packets called photons. The energy E carried by a photon is directly proportional to its frequency f:

$$E = h * f \tag{1}$$

Where h (J.s) is the Planck constant. Visible light or higher-energy light (ultraviolet) has enough energy to trigger the photovoltaic effect (Hernández-Callejo, Gallardo-Saavedra, & Alonso-Gómez, 2019).

At the heart of photovoltaic cells are semiconductor materials. The most commonly used one is silicon (Si). Semiconductors have a conductivity level between that of a good conductor (like metals) and an insulator. This allows their electrical properties to be controlled. Valence Band; the energy level where electrons are bound to atoms and normally cannot carry current. Conduction Band; the higher energy level where electrons can move freely and create an electric current. Band Gap; the energy difference between the valence band and the conduction band. This is the minimum energy barrier an electron must overcome to create a current (Husain & et al., 2018).

The photovoltaic effect occurs in a specially designed semiconductor assembly called the p-n junction. To increase and control the conductivity of a pure semiconductor, foreign atoms are added. In n-type semiconductor, when atoms with 5 valence electrons are added to silicon, 4 electrons form bonds with Si, and one electron is left free. In this region, electrons are the majority carriers (negative charge). In p-type semiconductor, when atoms with 3 valence electrons are added to silicon, a deficiency of an electron is created. This deficiency is called a "hole". In this region, holes are the majority carriers (positive charge) (Husain & et al., 2018).

The photovoltaic effect is shown schematically in Figure 1. The p-n junction is formed when n-type and p-type semiconductors are brought together. When the junction is formed, free electrons from the n-type side start diffusing into the p-type side, and holes from the p-type side diffuse into the n-type side. This movement creates a region right near the junction that is depleted of majority carriers. Electrons and holes neutralize each other in this area. As a result of the neutralization, positively charged ions remain on the n-side, and negatively charged ions remain on the p-side. This charge separation creates a permanent electric field across the junction, directed from the p-type side to the n-type side (Husain & et al., 2018).

Figure 1. Principle of the photovoltaic effect.

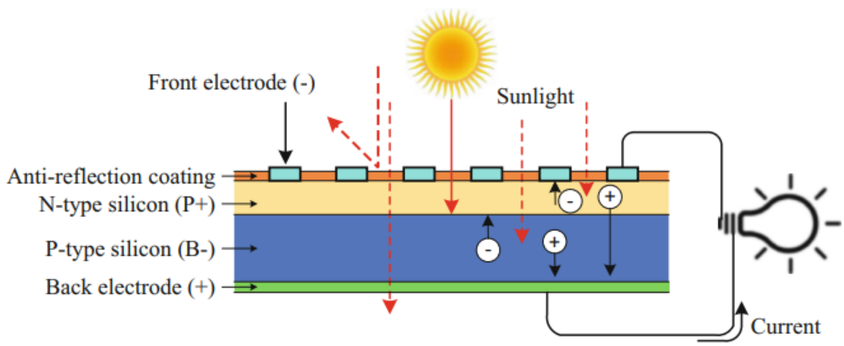

Source: (Yaman, & Eklas, 2022)

When sunlight (photons) strikes the solar cell, the photons transfer their energy to the electrons in the semiconductor material.

If the photon has sufficient energy (greater than the material's band gap), it knocks an electron loose from its atomic bond, creating an electron-hole pair. The electric field established across the p-n junction acts like a diode, sweeping the freed electrons toward the n-type layer and the holes toward the p-type layer. This separation of charge carriers is what creates a voltage. When an external circuit is connected to the metal contacts on the cell, the accumulated electrons flow through the circuit to the p-type layer to recombine with the holes, thus generating an electric current (DC). The overall efficiency of a solar cell is defined as the ratio of the electrical energy output to the solar energy input under standard test conditions.

Electrical Efficiency of a PV Module

The electrical efficiency (η) of a PV module is the single important metric for determining its performance. It quantifies how effectively the module converts the energy from incident sunlight into usable DC electrical power. PV module efficiency is mathematically defined as the ratio of the maximum electrical power output (P_{max}, W) to the total solar power incident on the module's area (A, m^2) under specific testing conditions (Alami & et al., 2016).

$$\eta = \frac{P_{max}}{E \times A} = \frac{I_{max} \times V_{max}}{E \times A} = \frac{J_{max} \times V_{max}}{E} \qquad (2)$$

In equation (2), E (W/m^2) is defined the total solar irradiance in the panel. The electrical efficiency of a PV module is a fundamental metric that critically affects the overall performance and design of a solar energy system. Since efficiency determines the ratio of maximum electrical power output to the total incident solar energy, it directly dictates the power density of the panel. Higher efficiency modules produce significantly more power than lower-efficiency panels of the exact same physical size, leading to a greater total energy yield (kWh) over the system's lifespan. This relationship is crucial where installation space is limited, such as on residential rooftops, because higher-efficiency modules allow system installers to achieve the target system capacity using fewer modules or a smaller total area. Furthermore, module efficiency impacts heat management; lower efficiency means a greater percentage of absorbed solar energy is wasted as heat, which raises the cell temperature. Since the electrical output voltage of silicon cells decreases with increasing temperature, this heat acceleration can negatively impact the short-term power output and potentially accelerate the degradation of the module's materials over the long term. Therefore, maximizing electrical efficiency is key to optimizing energy generation per unit of space and ensuring robust long-term performance.

Structure of PV Module

A PV module is a layered structure designed to convert sunlight into electricity while protecting the delicate internal components from the environment. In a PV module, the solar cell layer is enclosed and protected by two different encapsulant layers on both its front and back surfaces. Figure 2 indicates the layers of the standard PV module.

The glass layer is the topmost surface of the solar panel. It has two main functions such as protection and light transmission. It acts as the primary defense, protecting the solar cells from harsh environmental elements like rain, snow, hail, dust, and wind. It must be made of tempered, low-iron glass to maximize the amount of sunlight that passes through to the cells, maintaining high light transmittance (often over 91.5%). The tempering process adds strength and resistance to mechanical stress.

The encapsulant is a protective, adhesive film, typically made of Ethylene Vinyl Acetate (EVA) or similar polymers. There are usually two layers of encapsulant, one above and one below the solar cells. It acts like a glue, bonding the solar cells to the front glass and the rear backsheet, providing structural integrity. It also cushions the cells against mechanical stress and vibration. It seals the cells, preventing moisture and oxygen from reaching them, which could cause corrosion and degrade performance. In addition, it provides electrical insulation for the solar cells and their interconnections.

Figure 2. The layer of PV panel.

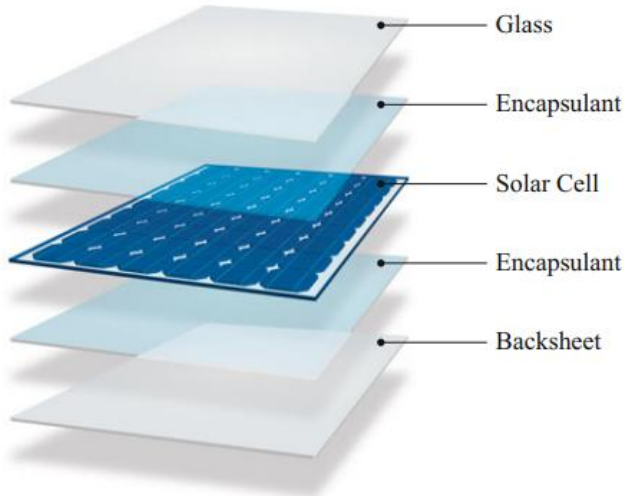

Source: (Yaman, & Eklas, 2022)

The solar cell layer is the core of the module where the magic happens. These cells (usually made of silicon, either monocrystalline or polycrystalline) use the photovoltaic effect to convert photons from sunlight directly into DC electricity. Individual cells are connected in series and parallel to achieve the desired voltage and current output for the entire module.

The backsheet forms the outermost rear layer of the PV module. It is a polymer (plastic) film, often made of materials like fluoropolymer. It serves as the second line of defense, protecting the cells and electrical components from moisture ingress, dust, and UV radiation from the rear. It also provides crucial electrical insulation between the internal circuitry and the mounting structure or ground, which is vital for safety. Moreover, it contributes to the overall structural support and rigidity of the modüle (Yaman, & Eklas, 2022).

Components of a PV System

A complete operational PV system, whether small-scale residential or large-scale utility, consists of several key components:

Photovoltaic Panels (Modules)

These are the primary components, consisting of multiple solar cells connected in series and parallel, encapsulated for protection, and framed (usually with aluminum) for structural integrity. The structure and key parts of a photovoltaic panel are shown in a simplified form in Figure 3.

Figure 3. The structure and key parts of the photovoltaic panel.

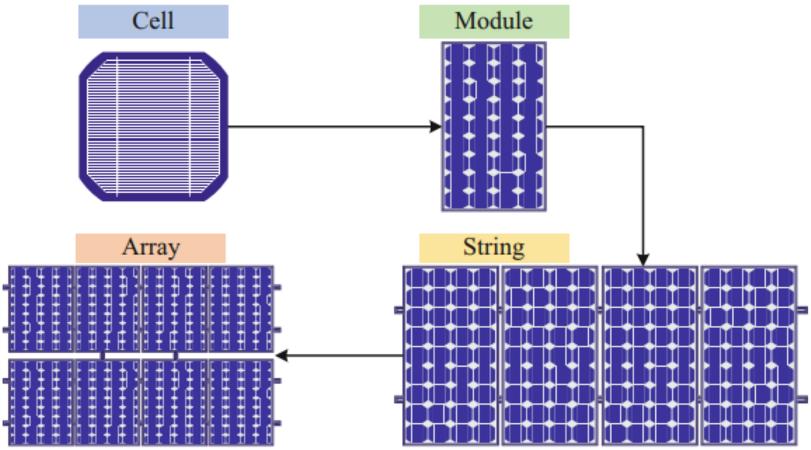

Source: (Yaman, & Eklas, 2022)

Inverter

An inverter is the most crucial component in a solar PV system after the solar panels themselves. Its primary function is to convert the Direct Current (DC) electricity produced by the solar panels into Alternating Current (AC) electricity, which is the standard power used by homes, businesses, and the main electrical grid. There are three main categories of inverter technology used today, each with its own advantages and setup:

String Inverters: These are the traditional and most common type of inverter. A string inverter is a single, central unit connected to a series of solar panels. All the DC power from the string of panels is fed into this one box, where it is converted into AC power. Generally the cheapest option for standard residential installations. Since it's a single unit, it's easier to access and diagnose issues. In addition, modern string inverters offer very high peak efficiencies (often 97-99%). However, the main drawback is that the entire string's performance is limited by the weakest panel. If even a small portion of one panel is shaded or dirty, the output of the entire string drops to the level of that underperforming panel. Typically, they only provide monitoring for the entire array, not for individual panels (Hoda & et al., 2019).

Micro-inverters: Installed under each individual panel, converting DC to AC at the module level. This maximizes energy harvest by mitigating the impact of shading on one panel from affecting the entire string. Micro-inverters completely mitigate the impact of shading. Since each panel operates independently, if one panel is shaded, the others continue to perform at full capacity. This is called Module-Level Power Electronics (MLPE). They offer panel-level monitoring, allowing homeowners to see the performance of every single panel. Also, it's easy to add more panels to the system later without changing the central equipment. But, the cost per watt is typically higher than a string inverter system because it is purchasing multiple smaller inverters. They are installed on the roof, making maintenance access slightly more difficult than a ground-level string inverter.

Power Optimizers: DC-to-DC converters installed at the module level that condition the DC power before sending it to a central string inverter. Power optimizers are a hybrid solution. They are DC-to-DC converters installed at the module level (like micro-inverters), but they do not convert to AC power. Instead, they condition the DC power, fixing the voltage and current, and then send the optimized DC power to a central string inverter. Power optimizers offer similar shading and mismatch benefits to micro-inverters, ensuring each panel operates at its maximum power point. Many brands include advanced safety features, like rapid shutdown capability, which is often required by building codes. They are generally cheaper than micro-inverters while offering most of the same performance benefits. However, it is still need both the optimizer at the panel level and a central string inverter, which can mean two points of potential failure. Figure 4 displays the layered structure and constituent parts of a PV modüle (Vincenzo & et al., 2020).

Figure 4. The components and structural layering of a photovoltaic module.

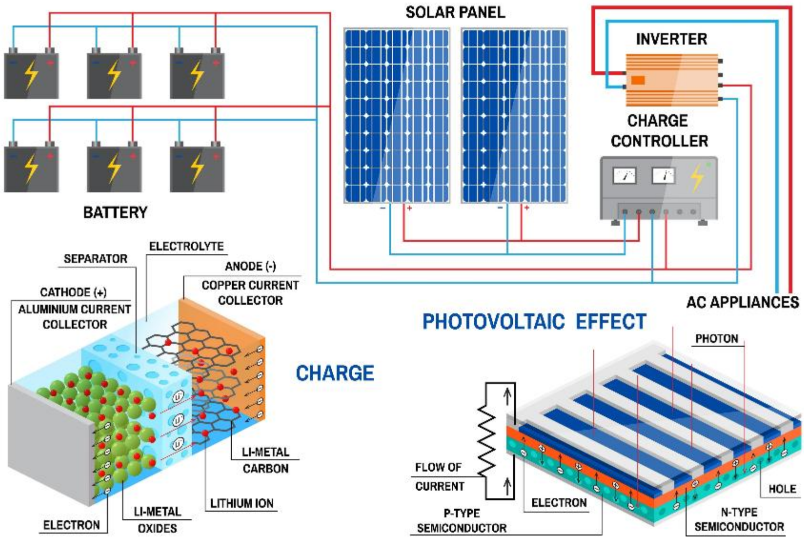

Mounting Structure and Racking

These are the mechanical components that hold the panels in place. They are designed to withstand wind and snow loads and are typically angled (tilt angle) and oriented (azimuth) to maximize sun exposure throughout the day and year.

This refers to the mechanical support system that physically secures the solar panels to the roof or ground. To hold the PV modules in a fixed, secure position and ensure they can withstand environmental stresses over their 25+ year lifespan. The structure must be engineered to resist high winds (uplift forces) and heavy snow accumulation (downward forces) common to the installation location.

Racking is most commonly made from anodized aluminum for its strength, low weight, and resistance to corrosion, though galvanized steel is also used for ground mounts. This is the compass direction the panels face. In the Northern Hemisphere, panels are ideally oriented due south to maximize total energy production. This is the angle of the panels relative to the horizontal plane. It is often set equal to the latitude of the location to maximize annual energy yield, but sometimes constrained by the pitch of the roof.

Attached directly to the roof structure. Free-standing systems anchored into the ground, often allowing for optimal tilt and azimuth regardless of structure. Used for smaller systems, where panels are mounted atop a single pole. Sophisticated systems that automatically adjust the panel's angle throughout the day to follow the sun's path, significantly increasing energy harvest (Hoda & et al., 2019).

Balance of System (BOS)

This includes all other components necessary for a complete, safe, and operational system, such as wiring, connectors, safety disconnect switches, fuses, junction boxes, and monitoring equipment.

The balance of system includes all the necessary components for a safe, operational, and complete solar PV installation, excluding the panels and the main inverter. These components start with wiring and conduits, which are the conductors that carry the generated DC and AC power between all parts of the system; the conduits serve to protect this wiring from environmental exposure and physical damage. Secure and reliable connections between the panels and other elements are ensured by connectors, most commonly the industry-standard MC4 plugs, which are weather-sealed.

For safety and maintenance, the system relies on safety disconnect switches that allow manual and immediate isolation of the solar array and/or the battery bank from the rest of the electrical system in emergencies or for servicing. Electrical protection is provided by fuses and circuit breakers, which are crucial overcurrent protection devices designed to prevent damage to the wiring and components from short circuits or power surges. Finally, the system utilizes junction boxes or combiner boxes enclosures where multiple strings of panels are electrically combined before the power is directed to the inverter. To track performance and ensure everything is running efficiently, monitoring equipment is used to track energy production and detect any faults (Hoda & et al., 2019; Vincenzo & et al., 2020).

Battery Storage

In off-grid systems or grid-tied systems with backup functionality, a battery bank stores excess energy generated during the day for use at night or during grid outages. Battery storage transforms a solar PV system from a simple power generator into an energy management system, allowing power to be used when the sun isn't shining. It can be store the excess DC energy generated by the solar panels during peak sunlight hours. This stored energy can then be discharged later. Mandatory for systems not connected to the electrical grid, providing the sole source of power at night and on cloudy days.

Provides power to critical loads during a utility grid outage. Allows homeowners to use their self-generated solar power during the evening peak demand hours when utility rates are highest, reducing their electricity bill. The most common technology for modern solar storage is Lithium-ion, replacing older lead-acid batteries due to their higher energy density, longer cycle life, and lower maintenance (Vincenzo & et al., 2020).

Types of Photovoltaic Technology

PV cells are broadly categorized into three generations based on the materials and manufacturing techniques used. Figure 5 illustrates the differences and classification of PV cells across the first, second, and third generations.

First Generation: Crystalline Silicon (c-Si)

This is the dominant and most mature technology in the global market, accounting for over 90% of current production. Silicon is abundant, non-toxic, and offers stable performance.

Monocrystalline Silicon (Mono-Si): Cells are cut from a single, pure, large crystal of silicon (grown using the Czochralski method). This uniformity results in less defects and higher electron mobility. Typically recognizable by their uniform dark color and rounded edges. Highest efficiency (often 20-23% for commercial modules) and better performance in low-light conditions. But, higher manufacturing cost due to the complex process of growing large single crystals; energy-intensive production.

Polycrystalline Silicon (Poly-Si or Multi-Si): Cells are made from blocks of silicon that consist of multiple crystals. The casting process is simpler and less expensive than mono-Si. Distinctive by their speckled, blue appearance due to the visible grain boundaries. Lower manufacturing cost and less silicon waste than mono-Si. However, slightly lower efficiency (typically 15-20%) because the multiple grain boundaries hinder electron flow (Alami, 2020).

Second Generation: Thin-Film Technologies

These technologies use minimal amounts of active material by depositing very thin layers (nanometers to micrometers thick) onto a substrate (like glass, plastic, or metal).

Amorphous Silicon (a-Si): Non-crystalline silicon deposited as a very thin layer. Often used in small-scale electronics and flexible solar panels. Cheaper to produce; flexible; good performance in high temperatures. Significantly lower efficiency than crystalline silicon; efficiency degrades slightly upon initial exposure to sunlight.

Cadmium Telluride (CdTe): A semiconductor compound of Cadmium and Tellurium. Dominant in the utility-scale thin-film market. Lowest manufacturing cost of any PV technology; fast manufacturing process; excellent performance in hot, sunny conditions. Contains the toxic heavy metal Cadmium; slightly lower efficiency than c-Si.

Copper Indium Gallium Selenide (CIGS): A compound semiconductor consisting of four elements. Used in modules that can be flexible or rigid. It offers some of the highest efficiencies among thin-film technologies (approaching c-Si performance) and has a uniform dark appearance. But, more complex and delicate manufacturing process; relies on less abundant metals (Indium and Gallium) (Alami, 2020).

Third Generation: Emerging Technologies

These technologies are still largely in the research and development phase, focusing on low-cost production, high theoretical efficiency, and unique applications.

Perovskites: A family of materials with a specific crystal structure. Research cells have rapidly achieved efficiencies competitive with silicon (over 25%). Can be manufactured using very low-cost solution processing and may enable highly efficient tandem cells. Poor long-term stability and degradation when exposed to moisture and heat.

Organic Photovoltaics (OPV): Uses carbon-based organic molecules or polymers. Extremely low cost, very lightweight, and highly flexible. Niche applications like integrated electronics, building façades, and wearable tech. Very low efficiency and short lifespan compared to traditional PV.

Quantum Dots and Dye-Sensitized Solar Cells (DSSC): Utilizing nanoscale materials or organic dyes to capture light, aiming for high efficiency in diverse light conditions and low production cost (Alami, 2020).

Figure 5. First, second, and third generation PV cell types.

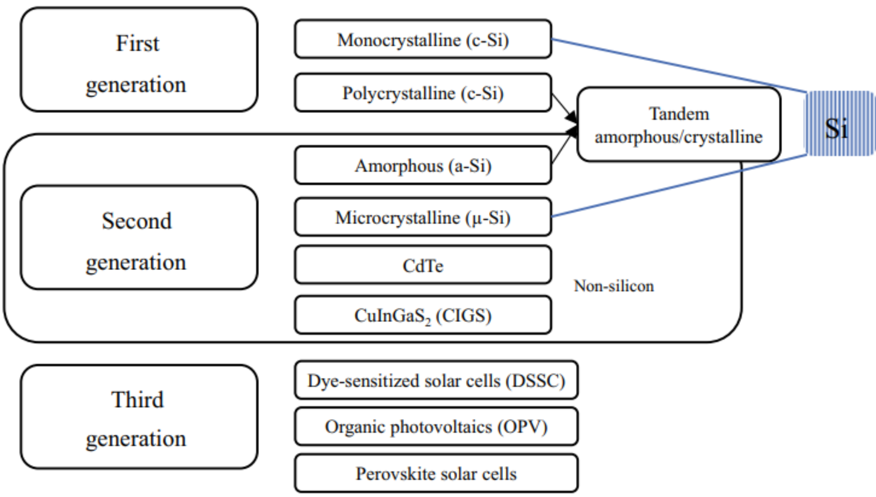

Source: (Alami, 2020)

Environmental and Economic Impact of PV Technology

The widespread adoption of PV technology has ushered in significant environmental benefits, primarily centered around combating climate change. By generating electricity directly from sunlight without any combustion, PV systems virtually eliminate the need to burn fossil fuels. This results in a drastic reduction in greenhouse gas (GHG) emissions, such as carbon dioxide (CO_2), which are the primary drivers of global warming. This shift to solar power directly contributes to achieving global climate targets and improving air quality by reducing pollutants such as sulfur dioxide and nitrogen oxides. Furthermore, the decentralized nature of solar generation can minimize transmission losses in long-distance power grids, thereby improving overall energy efficiency.

The economic implications of the PV revolution are equally profound, offering boosts to both national security and employment. For nations, solar power enhances energy security by reducing reliance on volatile, imported fossil fuels and diversifying the overall energy mix, which stabilizes the national grid. Economically, solar energy represents a form of deflationary energy. Once the substantial initial investment in hardware is made, the operational fuel (sunlight) is entirely free, leading to low and predictable long-term operating costs. This economic advantage is compounded by the phenomenon known as Swanson's Law, which states that the cost of solar cells tends to drop by 20% for every doubling of cumulative shipped volume. This dramatic cost reduction has made PV competitive with, and frequently cheaper than, conventional power generation sources globally. Crucially, the burgeoning solar industry acts as a powerful job creation engine, stimulating economies through the creation of new employment opportunities across manufacturing, sales, installation, and maintenance sectors.

Environmental Conditions on PV Panel Performance

The performance and efficiency of PV panels are critically dependent on the surrounding environmental conditions. While PV modules are designed to operate outdoors, fluctuations in weather, temperature, solar irradiance, and other factors significantly influence their electrical output and long-term durability. Understanding these effects is essential for accurate system sizing, performance prediction, and maintenance planning.

Temperature Effects

Temperature is arguably the most dominant environmental factor affecting PV performance. PV panels are typically rated under Standard Test Conditions (STC), which define a cell temperature of

25 °C. As the cell temperature rises above 25 °C, the open-circuit voltage of the panel decreases linearly. Since power is the product of voltage and current, this reduction in voltage directly causes a decrease in the overall maximum power output. This effect is quantified by the power temperature coefficient, usually expressed as a negative percentage per degree Celsius. This means for every degree Celsius rise above 25°C, the power output drops by the specified percentage. In real-world conditions, especially in hot climates, the Nominal Operating Cell Temperature (NOCT), which represents the cell temperature under 800 W/m^2 irradiance and 20 °C ambient temperature, is often used for a more realistic performance estimate. A panel operating in a hot summer environment can easily reach cell temperatures of 50 °C to 70 °C, leading to significant power derating (Muhammad, 2020).

Solar Irradiance (Intensity)

Solar irradiance, the amount of solar power received per unit area, is directly proportional to the current output and thus the power output of a PV panel. The short-circuit current of a PV panel is nearly linearly proportional to the intensity of the incident sunlight. High irradiance (e.g., above 1000 W/m^2 at STC) yields maximum current, while low irradiance, as on cloudy days, significantly reduces current and power. Irradiance is attenuated by various atmospheric conditions. Dense cloud cover can reduce irradiance to less than 10% of peak values. In addition, dust, smog, and other airborne particles scatter and absorb sunlight, reducing the energy reaching the panel surface. The air mass factor, which represents the optical path length the sun's rays must travel through the atmosphere, affects intensity. It is lowest at solar noon and highest (more scattering/absorption) near sunrise and sunset (Muhammad, 2020).

Soiling and Dust Accumulation

Soiling refers to the accumulation of dust, dirt, pollen, bird droppings, and other opaque materials on the panel surface. These particles block the sunlight from reaching the PV cells, effectively acting as partial shading. Even small amounts of dust can cause a measurable loss in energy yield. In dry, arid regions, power losses due to soiling can range from 1% to 5% daily. Uneven soiling can lead to partial shading of specific cells within the panel. This forces the shaded cells to operate in reverse bias, dissipating energy as heat instead of generating it, creating localized high-temperature areas known as hot spots. Hot spots can cause irreversible damage to the cell, encapsulant, and backsheet, severely reducing the panel's lifespan and output (Muhammad, 2020).

Wind and Airflow

Wind influences the panel's performance primarily through its cooling effect. Wind passing over the panel surface increases convective heat transfer, removing heat and keeping the cell temperature lower than it would be in still air. As established, lower cell temperatures lead to higher voltage and power output. Conversely, strong winds exert mechanical stress on the mounting structures and the panels themselves. Over time, constant wind loading can lead to micro-cracks in the PV cells, structural fatigue, and seal failures, reducing long-term reliability (Muhammad, 2020).

Humidity and Moisture

High humidity and direct moisture (rain, snow, dew) primarily impact the long-term reliability and degradation of the PV module. High voltage systems operating in humid environments can suffer from PID, a phenomenon where high potential differences between the cell and the frame cause charge leakage and significant power loss. Moisture penetration through minor defects in the edge sealing or backsheet can lead to corrosion of the metallic components (like cell interconnections and contacts), which degrades the electrical performance. Rain or snow, while initially washing away some dust, can also leave behind water spots or mineral residues after evaporation, which contribute to soiling (Muhammad, 2020).

Snow and Icing

In cold climates, snow and ice pose a physical obstruction to sunlight. A layer of snow or ice completely covering the panel surface effectively cuts off all solar irradiation, resulting in zero power output. The panel's tilt angle and mounting height are crucial for natural snow shedding. Steeper angles aid in the natural slide-off of snow. When snow covers the ground around the panels but not the panels themselves, the high albedo (reflectivity) of the snow can increase the amount of sunlight reflected onto the panels. This can occasionally boost the irradiance and power output, provided the cell temperature remains low (Muhammad, 2020).

Studies in The Literature on Environmental Conditions in PV Panel Performance

Maximum Power Point Tracking (MPPT) is crucial for PV systems, ensuring they extract the maximum available power despite fluctuating atmospheric conditions. The suitability of an MPPT technique is determined by factors like speed of convergence, accuracy, and efficiency. Among the various methods, hill-climbing algorithms are widely used in commercial applications. Jately & Arora researced an efficient dual-tracking MPPT technique designed for rapidly changing conditions. A comparative performance analysis in Matlab/Simulink and a comparison of energy yield under a typical one-day irradiance profile validated the proposed dual-tracking technique and demonstrate its economic advantage (Jately & Arora, 2017). Humairi et al. analyzed the features and characteristics of real-world PV system data collected from a solar facility in Oman to investigate the relationship between soiling accumulation and solar panel performance. Leveraging a large dataset of 36,851 observations of various environmental and operational parameters, the researchers conducted extensive mathematical and statistical analyses to accurately model and understand the data dynamics. The study's key findings deepened the understanding of PV system data features and clearly revealed the detrimental influence of soiling on energy output, emphasizing the need to consider geographical and climatic variations. Ultimately, the research provided actionable insights for optimizing the performance and reliability of PV installations in real-world settings (Al Humairi, 2024). Talaat et al. proposed a hybrid modeling approach using Artificial Neural Networks (ANNs) optimized with Multiverse Optimization (MVO) and a Genetic Algorithm (GA) to accurately predict PV output power, efficiency, and cell temperature. The Multilayer Feedforward Neural Network (MFFNN) structure was optimized by MVO and GA to improve the ANN's weights, biases, and neuron counts, using two years of data from a 4-kW PV plant in Shaqra City, Saudi Arabia. The models rely on ambient temperature, wind speed, and solar irradiance as inputs, and the MFFNN-MVO model showed superior accuracy in predicting PV efficiency, achieving a low Normalized Root Mean Square Error (NRMSE) of $2.82E^{-4}$. The research also investigated the strong dependency of PV efficiency on cell temperature, highlighting the importance of the temperature factor (Talaat, Said, Mohamed & Essa, 2022).

Bonie et al. created a dataset to characterize the performance of PV panels under various fault conditions, including discoloration, cracks, and partial shading. As seen in Figure 6, testing was conducted under three scenarios - dirty, clean, and partially shaded surfaces- measuring electrical parameters (like short-circuit current and output power) and capturing thermographic images. The results confirmed that faults and partial shading lead to a notable reduction in power production, providing valuable real-world data for researchers focused on fault detection, maintenance optimization, and enhancing the overall efficiency of solar energy systems (Bonie & et al., 2025).

Figure 6. (a) Clean, (b) Dirty, and (c) under Partial Shading condition.

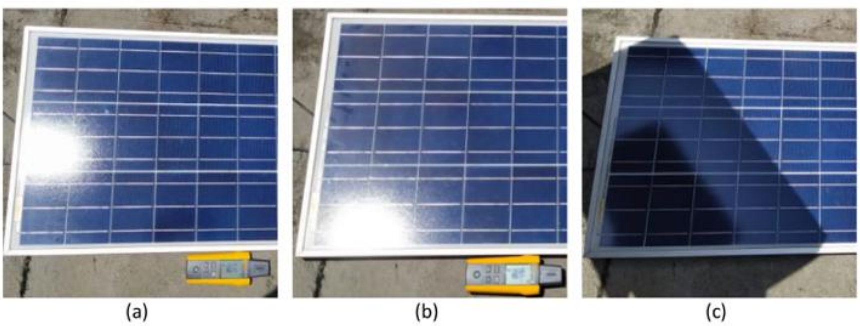

Source: (Bonie & et al., 2025)

Salam et al. developed a new, flexible PV panel model within the Proteus software environment to accurately forecast and evaluate the impact of environmental factors like irradiance and temperature on PV performance. The model was based on the mathematical equations of a single-diode equivalent circuit (including photo-generated, shunt-resistor, and diode currents) and is built using Proteus's "Pick Devices." The proposed model's effectiveness was validated by applying it to monocrystalline and multi-crystalline silicon cells and comparing the resulting I-V and P-V characteristic curves with manufacturer data, PVsyst software, and other research. The simulation confirmed that the model is simple, flexible, and suitable for diverse PV technologies under various weather conditions (Salam, Yaqoob & Ephraim, 2022). Zlateva et al. researched the severe impact of limestone dust accumulation on PV panel performance, specifically focusing on sites near quarries (see Figure 7). Field measurements demonstrated that the high concentration of limestone dust accumulates rapidly and, when mixed with moisture, forms a hard, resistant layer that was difficult to remove even with moderate rain or wind. The study revealed that a lack of systematic cleaning could lead to a significant drop in efficiency of over 20%, severely limiting the return on investment. This research underscored the critical need for innovative maintenance strategies, such as regular cleaning, special coatings, and design adaptation, for PV systems in highly polluted, dusty environments (Zlateva & et al, 2020).

Yaxin et al. addressed the critical issue of PV system reliability loss due to dust accumulation and temperature rise, which significantly reduced energy efficiency. It proposed a mathematical modeling approach to determine the optimal cleaning frequency. The model employed a Non-homogeneous Compound Poisson Process (NHCPP) for dust and Markov chains for temperature evolution, incorporating environmental factors like wind and rainfall as covariates. The study introduced and evaluated a Condition-based cleaning policy, determining optimal thresholds to minimize the long-term average maintenance cost. Numerical results showed that non-periodic inspections offered a performance gain ranging from

3.83% to 9.37% over periodic inspections (Yaxin, Mitra & Antoine, 2024).

Figure 7. Visual characteristic of a PV panel contaminated with limestone dust and the establishment of resistance to the accumulated dust layer.

Source: (Zlateva & et al, 2020: 11)

In the another study, Indrojeet et al. proposed an OFF-Grid PV-Battery stand-alone system featuring an enhanced DC-DC boost converter and an efficient voltage balancing technique. The converter achieved the required high-voltage gain at a lower duty ratio, significantly reducing the voltage stress on the switching devices compared to conventional topologies. The system utilized the incremental conductance technique for MPPT and included a simple technique to maintain a constant DC bus voltage with a fast dynamic response. Designed to handle a 1 kW load at 180 V, the system demonstrates high reliability and an overall efficiency of around 93% under varying input and load conditions (Indrojeet, Sreejith, & Sovit, 2022).

Chao et al. investigated the PV Nexus Cleaning Recommendation System (PNCRS), an intelligent cleaning recommendation system designed to optimize PV panel cleaning schedules, addressing the inadequacies of traditional fixed-interval methods in fluctuating environmental conditions. The PNCRS utilized data augmentation and Wavelet Packet Energy Transmissibility Function (WPETF) to handle sparse data and reduce dependency on irrelevant features, enhancing real-time environmental adaptability. Furthermore, it employed profit-based Bayesian Optimization to dynamically adjust model weights for comprehensive profit optimization. Evaluation across two distinct PV farms validated the system's effectiveness, demonstrating significant profit increases of 29% and 34%, underscoring its superiority over conventional cleaning strategies (Chao & et al. 2025). Abhishek et al. introduced a comparative machine learning approach using Multivariate Regression (MR), Support Vector Machine Regression (SVMR), and Gaussian Regression (GR) to precisely predict solar PV panel power output based on environmental factors like solar radiation, temperature, and humidity. The results showed that the SVMR model was superior, achieving exceptional performance with an R^2 value of 0.99, significantly outperforming the GR model, which yielded an R^2 of 0.88. This high accuracy highlighted SVMR's reliability in forecasting PV output, which had significant implications for optimizing PV panel deployment and accelerating the adoption of solar power in diverse environmental conditions. The research offered valuable insights into how PV power generation adapts to changing weather, contributing to the expansion of solar energy (Abhishek & et al., 2025).

Conclusion

This study thoroughly explored the multifaceted world of PV panels, ranging from the fundamental physics governing their operation to the critical environmental and economic factors influencing their deployment and performance. We began by demystifying the physics behind the photovoltaic effect, establishing how light energy is directly converted into electrical energy via the excitation of electrons in semiconductor materials. This foundational understanding paved the way for analyzing the electrical efficiency of a PV module, emphasizing key metrics like the fill factor and maximum power point, which define a panel's true power output potential.

A deeper dive into the system revealed the intricate structure of a PV module, including protective layers, encapsulation, and the cell arrangement, all designed for durability and optimal light absorption. We then expanded our scope to the complete energy harvesting system, detailing the essential components of a PV system such as inverters, mounting structures, and wiring that are necessary to convert DC power into usable AC electricity and safely integrate it into the grid or a local load. Furthermore, a comparison of the different types of photovoltaic technology including crystalline silicon (mono/polycrystalline), thin-film (CdTe, CIGS, a-Si), and emerging perovskites highlighted the continuous innovation aimed at improving efficiency, reducing cost, and broadening applicability.

The discussion then shifted to the broader implications, assessing the significant environmental and economic ımpact of PV technology. Economically, PV has proven to be a rapidly maturing technology, achieving cost parity or even advantage over traditional fossil fuels in many regions. Environmentally, despite the energy required for manufacturing, the long-term operation of PV systems offers substantial benefits by generating clean electricity, reducing greenhouse gas emissions, and decreasing reliance on finite resources, solidifying its role in a sustainable energy future.

Crucially, the performance of these systems is inextricably linked to their surroundings, as highlighted in the section on environmental conditions on PV panel performance. Variables like solar irradiance, ambient temperature, wind speed, and soiling were identified as primary factors affecting power output. Elevated temperatures, for instance, significantly degrade voltage and power output, necessitating careful thermal management and panel selection. Conversely, optimal cleaning and reduced shading ensure that the panel receives the maximum possible solar resource. Ultimately, the transition to widespread PV adoption requires not only technological advancement but also site-specific analysis, careful installation, and proactive maintenance to mitigate these environmental challenges. The integration of PV technology, supported by smart grid solutions and energy storage, is paramount for securing a resilient and decarbonized energy supply for the future.

According to the extensive review of literature, studies consistently highlight that fluctuations in irradiance, ambient temperature, and the physical degradation caused by soiling and other faults are the primary determinants of actual energy yield. The challenge is not merely to generate power, but to sustain maximum power extraction under diverse, non-ideal, and often rapidly changing atmospheric conditions. The research presented here demonstrates a clear, continuous effort within the PV sector to develop advanced techniques ranging from improved electrical models to intelligent maintenance systems to counteract these environmental adversities and maximize the economic viability of solar energy. A significant focus in recent research has been on the development of sophisticated control and modeling techniques.

In summary, the literature reviewed confirms that the path to truly efficient and reliable PV energy lies in a holistic integration of robust electrical engineering, data science, and condition-based optimization. While advanced MPPT and converter designs ensure high electrical efficiency, the intelligent management of environmental degradation through predictive modeling and optimized cleaning schedules is equally crucial for long-term economic returns. Future research should continue to focus on creating more adaptive, self-correcting systems that can dynamically respond to diverse climatic profiles, ensuring solar energy remains a globally viable and expanding power source.

References

Abhishek, K.T., Mangalpady, A., Elumalai, P.V., Krishnasamy, K., A. Shern, K., Mohammad, A. & Koppula, S.R. (2024). Advancing solar PV panel power prediction: A comparative machine learning approach in fluctuating environmental conditions. *Case Studies in Thermal Engineering,* 59, 104459. Doi: 10.1016/j.csite.2024.104459.

Aktaş, A., Koşan, M., Aktekeli, B., Güven, Y., Arslan, E. & Aktaş, M. (2024). Numerical and experimental investigation of a single-body PVT using a variable air volume control algorithm. *Energy*, 307, 132793. Doi: 10.1016/j.energy.2024.132793.

Alami, A. H., Abed, J., Almheiri M., Alketbi, A. & Aokal, C. (2016). Fe-Cu metastable material as a mesoporous layer for dye-sensitized solar cells. *Energy Science Engineering*, 4(2), 166-179. Doi: 10.1002/ese3.114.

Alami, A.H. (2020). *Introduction to mechanical energy storage. In Mechanical energy storage for renewable and sustainable energy resources*. Switzerland: Springer International Publishing, 1–12. Doi: 10.1007/978-3-030-33788-9_1.

Al Humairi, A., El Asri, H. Al Hemyari, Z.A. & Jung, P. (2024). Assessing the Features of PV System's Data and the Soiling Effects on PV System's Performance Based on the Field Data. *Energies*, 17, 4419. Doi: 10.3390/en17174419.

Arslan, E., Can Ö. F., Koşan, M. Demirtaş, M. Aktekeli B. & Aktaş, M. (2023). Numerical and experimental assessment of a photovoltaic thermal collector using variable air volume. *Thermal Science and Engineering Progress*, 39, 101735. Doi: 10.1016/j.tsep.2023.101735.

Bonie, J. R. Cristian, G. L. John, A. M. & Jhon, M. (2025). Dataset of photovoltaic panel performance under different fault conditions cracks, discoloration, and shading effects. *Data in Brief*, 59, 111392. Doi: 10.1016/j.dib.2025.111392.

Chao, Z., Yunfeng, M., Guolin, Y. & Tao, C. (2025). An integrated industrial PV panel cleaning recommendation system for optimal dust removal. *Applied Energy*, 377, 124692. Doi: 10.1016/j.apenergy.2024.124692.

Hernández-Callejo, L., Gallardo-Saavedra, S. & Alonso-Gómez, V. (2019). A review of photovoltaic systems: Design, operation and maintenance. *Solar Energy*, 188, 426-440. Doi: 10.1016/j.solener.2019.06.017.

Hoda, A., Maria, C., Browne, O. Anita, J. H., Ming, J. N., Hewitt, N. & McCormack, S. J. (2019). Efficient energy storage technologies for photovoltaic systems. *Solar Energy*, 192, 144-168. Doi: 10.1016/j.solener.2018.03.052.

Husain, A. F. W., Hasan, W. Z., Shafie S., Hamidon, M. N. & Pandey, S. S. (2018). A review of transparent solar photovoltaic Technologies. *Renewable and Sustainable Energy Reviews*, 94, 779-791. Doi: 10.1016/j.rser.2018.06.031.

Indrojeet, C., Sreejith, S. & Sovit, K.P. (2022). An enhanced DC-DC boost converter based stand-alone PV-Battery OFF-Grid system with voltage balancing capability for fluctuating environmental and load conditions. *Energy Sources, Part A: Recovery, Utilization, and Environmental Effects*, 44(3), 8247-8265. Doi: 10.1080/15567036.2022.2120574.

Jately, V. & Arora, S. (2017). Development of a dual-tracking technique for extracting maximum power from PV systems under rapidly changing environmental conditions. *Energy*, 133, 557-571. Doi: 10.1016/j.energy.2017.05.049.

Muhammad, T., Amani, A., Feras, K., Emad, A., Fares, A. & Malek, A. (2021). Environmental impacts of solar photovoltaic systems: A critical review of recent progress and future Outlook. *Science of The Total Environment*, 759, 143528. Doi: 10.1016/j.scitotenv.2020.143528.

Notton, G., Cristofari, C., Mattei, M. & Poggi, P. (2005). Modelling a double-glass photovoltaic module using finite differences. *Applied Thermal Engineering*, 25, 2854–77. Doi: 10.1016/j.applthermaleng.2005.02.008.

Parida, B., Iniyan, S. & Goic, R. (2011). A review of solar photovoltaic Technologies. *Renewable and Sustainable Energy Reviews*, 15, 1625–36. Doi: 10.1016/j.rser.2010.11.032.

Skoplaki, E. & Palyvos, J. A. (2009). Operating temperature of photovoltaic modules: a survey of pertinent correlations. *Renewable Energy*, 34, 23–9. Doi: 10.1016/j.renene.2008.04.009.

Salam, J., Yaqoob, S. M. & Ephraim, B. A. (2022). A new model for a photovoltaic panel using Proteus software tool under arbitrary environmental conditions. *Journal of Cleaner Production*, 333, 130074. Doi: 10.1016/j.jclepro.2021.130074.

Talaat, M., Said, T., Mohamed, A. & Essa A.Y., (2022). Hatata, Integrated MFFNN-MVO approach for PV solar power forecasting considering thermal effects and environmental conditions. *International Journal of Electrical Power and Energy Systems*, 135, 107570. Doi: 10.1016/j.ijepes.2021.107570.

Vincenzo, M., Maurizi, C., Domenico, C., Mistretta, M. & Maria, L. P. (2020). Review on Life Cycle Assessment of Solar Photovoltaic Panels. *Energies*, 13(1), 252 Doi: 10.3390/en13010252.

Yaman, A. J. & Eklas, H. (2022). *Photovoltaic Systems Fundamentals and Applications*. Switzerland: Springer Nature. Doi: 10.1007/978-3-030-89780-2_5.

Yaxin, S., Mitra, F. & Antoine, G. (2024). Impact of dust and temperature on photovoltaic panel performance: A model-based approach to determine optimal cleaning frequency. *Heliyon*, 10(16), e35390. Doi: 10.1016/j.heliyon.2024.e35390.

Zlateva, P., Terziev, A., Yordanov, K., Ivanov, M. & Stankov, B. (2025). Influence of Limestone Duston PV Panel Efficiency in a Small Solar Park in Bulgaria. *Engineering Data*, 6, 10. Doi: 10.3390/eng6010010.

DARRIEUS VERTICAL AXIS WIND TURBINES WITH AUXILIARY BLADES: A STATE-OF-THE-ART REVIEW AND SYNTHESIS OF DESIGN PRINCIPLES

Introduction

The global intensification of economic growth, industrial development, and socio-economic welfare has driven a pronounced acceleration in worldwide energy consumption (Acir et al., 2021; Acır et al., 2019; S. Kumar & Rathore, 2023; Acır & Tanürün, 2019). Over the past five decades, increases in per-capita income and urbanization have driven unprecedented growth in electricity consumption, transportation needs, and energy-intensive manufacturing (S. Kumar & Rathore, 2023). While economic and technological advancement depend on secure and affordable energy supplies, the structure of current energy generation remains highly dependent on fossil fuels (Asif & Muneer, 2007; Kabeyi & Olanrewaju, 2022). In most regions, conventional energy systems continue to be dominated by coal, petroleum, and natural gas, which together supply the majority of global primary energy demand (Seyhan et al., 2025; Tanürün et al., 2019). The persistence of fossil-fuel dependence has introduced structural vulnerabilities across environmental, social, and economic dimensions (Exner et al., 2016; D. Zhang et al., 2017). The most widely recognized challenge arises from greenhouse gas (GHG) emissions, predominantly carbon dioxide and methane, which accelerate global warming and intensify environmental hazards. Air quality degradation resulting from combustion products poses severe risks to public health (Seifi Davari, Mihaela Botez, et al., 2024), ecosystems, and agricultural productivity (Tanürün, 2023c). Fossil fuel supply chains also generate extensive environmental contamination associated with extraction, refining, and transportation. Another systemic challenge is resource depletion: fossil energy resources are finite (Ata et al., 2022; Seifi Davari, Seify Davari, & Ntantis, 2025), geographically concentrated, and increasingly difficult to extract, leading to higher operational risks, environmental damage, and economic volatility. In addition to environmental and economic risks, fossil-based energy infrastructures exhibit complex dependencies that compromise national energy security (McCollum et al., 2013). Countries without domestic fossil resources face import reliance, trade deficits, and exposure to market fluctuations, while exporting countries struggle with economic diversification and revenue fragility. These structural weaknesses highlight the urgency of energy transition strategies that emphasize sustainability, security, and resilience.

In this context, renewable energy technologies have emerged as key components in decarbonization, energy security enhancement, and long-term sustainable development (Hoseinzadeh et al., 2023; Tanürün, 2023b). Renewable energy systems, such as wind, solar, hydropower, bioenergy, and geothermal, offer multiple advantages over fossil-based systems. Among their most widely acknowledged benefits are: (i) reduced GHG emissions; (ii) improved local air quality; (iii) long-term resource availability; (iv) strengthened national energy independence; (v) reduced operational and marginal electricity costs; and (vi) reduced long-term economic externalities (Tanürün, 2023a). Renewable energy systems also exhibit modularity, scalability, and compatibility with distributed generation paradigms, enabling integration into future smart-grid infrastructures. Despite widespread deployment, many renewable energy technologies are no longer considered emergent or experimental; rather, they are recognized as technically robust and economically competitive electricity generation systems. Over the last two decades, advancements in materials engineering, aerodynamics, power electronics, control systems, and grid integration have driven rapid cost reductions and efficiency improvements, allowing renewables to compete with or even outperform conventional energy sources in many markets. Among the diverse renewable energy technologies currently deployed, wind energy has achieved particular prominence (Alanis Ruiz et al., 2021) due to its operational maturity, technological reliability, and proven capacity for both large-scale and distributed electricity generation.

Wind energy technologies can broadly be categorized into two configurations based on rotor axis orientation: horizontal-axis wind turbines (HAWTs) and vertical-axis wind turbines (VAWTs) (Bhuyan & Biswas, 2014; Salman et al., 2019). Historically, the wind industry has been dominated by HAWT designs, particularly three-bladed, upwind configurations, which have achieved a high level of technological standardization (Seifi Davari, Botez, et al., 2024b; Tanürün, 2023e). HAWTs offer high aerodynamic efficiency and scalability, enabling deployment in utility-scale wind farms that generate hundreds of megawatts (Seyhan & Tanürün, 2024). Their rotor-aligned operation allows blades to operate closer to optimal angles of attack, thereby supporting higher effective lift-to-drag ratios. In parallel, blade optimization techniques have matured to yield substantial energy conversion efficiencies. Consequently, HAWTs continue to represent the predominant commercial technology in global wind energy markets (Liu et al., 2019). Nevertheless, HAWTs exhibit several structural, environmental, and functional drawbacks that limit their deployment flexibility. First, HAWTs require active yaw control systems to continuously orient the rotor into the prevailing wind direction (Tanürün, 2023d). This mechanism increases mechanical complexity, maintenance requirements, and overall cost. Second, HAWTs are highly sensitive to spatial variability in wind speed, necessitating installation at elevated hub heights supported by tall towers to access stronger and less turbulent wind regimes. These towers impose engineering challenges, substantially increase capital expenditure, and restrict deployment in highly populated environments (Koşan et al., 2024). Third, HAWTs may produce elevated noise levels due to blade-tip vortices, trailing-edge turbulence, and inflow fluctuations, which limit their compatibility with residential or low-noise environments. Fourth, large-scale installations introduce ecological risks, including potential disruption of bird populations (Z. Wang & Zhuang, 2017), habitat fragmentation (Y. Wang et al., 2016), and increased collision rates (Tanürün, 2025b). Consequently, while HAWTs offer high energy yield and commercial reliability, they are constrained by environmental, mechanical, and infrastructural complexities.

VAWTs present a structurally and operationally distinct alternative, categorized primarily into two aerodynamic types: Darrieus (lift-based) and Savonius (drag-based) rotors (Ghafoorian et al., 2025; Kaya et al., 2022; Seifi Davari, Botez, et al., 2024a). In recent years, the Darrieus VAWT configuration has attracted significant research attention due to its self-supporting geometry, omnidirectional wind capture (Guo et al., 2019), and favorable structural characteristics. Unlike HAWTs, Darrieus VAWTs do not require active yaw systems (Tanürün & Acır, 2022), as their rotational symmetry allows them to operate effectively regardless of wind direction. Additional advantages include reduced acoustic emissions (Abdel-razak et al., 2026; Su et al., 2020a), lower center of gravity (Tanürün, 2025a), simplified generator integration, and enhanced structural resilience due to distributed load characteristics (Rezaeiha et al., 2018). Moreover, the compact rotor layout and short tower requirements enable compact system integration (Al-Hadhrami, 2014), favorable scalability characteristics (Paraschivoiu, 2009), and ease of installation (Seifi Davari, Seify Davari, Botez, et al., 2025; Z. Xu et al., 2018), particularly in constrained built environments. Because VAWTs operate efficiently at lower hub heights, they can be deployed closer to the ground (Rezaeiha et al., 2017), enabling lower maintenance costs and improved accessibility for inspection and servicing. VAWTs also demonstrate relatively strong performance in turbulent conditions (Azadani, 2023; X. Wang et al., 2025), making them suitable for urban settings (Bianchini et al., 2015) where wind direction fluctuates rapidly, noise constraints are critical, and turbine height is restricted.

Furthermore, the compact form factor and simplified tower requirements of VAWTs facilitate integration into distributed and community-scale energy systems, including building-mounted, rooftop, and ground-level installations (van Hooff et al., 2011). Urban wind energy development is increasingly recognized as a complementary pathway for local electricity generation, grid resilience, and energy decentralization (Davari et al., 2024). In this context, the deployment of VAWTs is technologically aligned with architectural constraints, social acceptance, and environmental sustainability. Despite these advantages, Darrieus VAWTs face two critical aerodynamic challenges: low power density and poor self-starting capability (Li et al., 2018; Seifi Davari et al., 2023; Su et al., 2020b). Lift-based rotors often require an initial external torque source or minimum wind speed to overcome static stall, resulting in unsteady operational behavior and extended cut-in periods. Additionally, the transient and unsteady aerodynamic environment associated with rotating, curved blades induces dynamic stall phenomena, flow separation, and cyclic load variation, collectively contributing to reduced mean power output. These performance constraints have motivated intensive research toward performance enhancement strategies, with a particular emphasis on aerodynamic control methodologies.

Flow-control systems have emerged as a central research direction for improving the aerodynamic performance of wind turbines, particularly VAWTs operating at low Reynolds-numbers. Flow-control methods aim to manipulate boundary-layer behavior, delay separation, regulate wake dynamics, and improve lift characteristics while minimizing drag penalties. These methods are classified into two general categories: active flow-control (AFC) and passive flow-control (PFC) (Gad-el-Hak, 2012; Tanürün, 2025c). Active systems typically include dielectric barrier discharge (Fadaei et al., 2021; Zavarian et al., 2023), synthetic jets (Kutluca et al., 2023; Matiz-Chicacausa et al., 2023), plasma actuators (Benmoussa & Páscoa, 2023; J. Xu et al., 2025), and blowing/suction devices (Sun et al., 2024; L. Wang et al., 2022). Although effective in flow manipulation, active systems impose additional complexity due to their dependence on external energy input, specialized electronics, and continuous actuation mechanisms, which constrain their scalability, robustness, and economic viability. Conversely, PFC techniques operate without external power input (Tanürün et al., 2024), relying primarily on geometric or surface features to manipulate aerodynamic structures. PFC systems are often preferred due to their structural simplicity, mechanical reliability, low manufacturing cost, and ease of implementation. PFC strategies are designed to suppress or delay boundary-layer separation, promote reattachment, and control vortex shedding via structural modifications (Yildiz et al., 2025). Examples include vortex generators (VGs) (Fouatih et al., 2016; H. Wang et al., 2017), riblets (Tanürün et al., 2021), backward-facing steps (Aziz et al., 2024; Mishriky & Walsh, 2016), surface cavities (Ibrahim et al., 2022; Yousefi Roshan et al., 2021), roughness (C. Zhu et al., 2022), leading-edge tubercles (Ke et al., 2022; Tanürün & Acır, 2019), slotted (Tanürün et al., 2026; Yıldız et al., 2025), J-shaped (Mirmotahari et al., 2025; Zamani et al., 2016), auxiliary blades (Asadbeigi et al., 2023; Li et al., 2022), and flap-type add-ons such as Gurney (Çakıroğlu et al., 2023; H. Zhu et al., 2021), adaptive (Hao et al., 2021; Tanürün, 2024) and split-flaps (L. Zhang et al., 2021). Collectively, these devices aim to alter flow topology, enhance circulation, and stabilize unsteady aerodynamic phenomena, resulting in improved torque production and energy conversion.

Among these techniques, auxiliary blade systems have gained increasing research attention due to their capacity to redistribute aerodynamic loads, modify local flow structures, and influence wake behavior with minimal geometric intrusion. Auxiliary blades function as supplementary lifting surfaces that augment the effective camber or alter pressure gradients, thereby improving aerodynamic performance in low-Re, unsteady flow environments. Their integration is particularly attractive for VAWTs, where stall dynamics and unsteady flow structures dominate performance limitations. Despite the increasing research devoted to auxiliary blade implementations in VAWTs, current literature remains methodologically dispersed, often restricted to specific geometries, narrow operating conditions, or case-specific experimental or numerical investigations. At present, there is no focused synthesis that evaluates auxiliary blade technologies specifically within the context of Darrieus-type VAWTs, particularly with respect to their aerodynamic mechanisms, performance implications, and design constraints. Accordingly, a targeted review of auxiliary blade systems for Darrieus rotors is needed to consolidate available findings, highlight performance trends, and delineate research gaps relevant to low-Reynolds-number VAWT operation. In this context, the present study conducts a structured review of auxiliary blade applications for Darrieus VAWTs. The review surveys existing computational, and experimental studies, summarize aerodynamic effects reported in the literature, and assesses their relevance to performance enhancement under unsteady, rotating-blade flow conditions. Rather than aiming to provide a universal framework, this work emphasizes the specific mechanisms and limitations associated with auxiliary blade configurations in Darrieus rotors, with the objective of identifying unresolved challenges and potential directions for future research in PFC design for VAWTs.

Auxiliary Blade Applications

Auxiliary blades are supplementary aerodynamic surfaces mounted on the primary rotor blade, designed to alter the rotor's aerodynamic characteristics by reducing flow separation, modifying pressure distribution, and redistributing aerodynamic loads, thereby improving overall performance. Numerical simulations have shown that, with appropriate placement and optimized thickness and attachment angle, an auxiliary blade can yield noticeable improvements in both starting torque and power coefficient (C_P) in Darrieus-type VAWTs (Li et al., 2019). Consequently, auxiliary blade configurations have received considerable attention in vertical-axis (particularly Darrieus) wind turbines, where low Reynolds number operation, unsteady wind inflow, and variable angle of incidence impose substantial performance limitations. Under such conditions, auxiliary blades offer promising potential for enhancing starting torque, expanding the operational range, and improving energy conversion efficiency (Uma Reddy et al., 2023). These improvements have prompted extensive research on auxiliary blade configurations in the literatüre over the past few years.

Li et al. (2016) proposed a novel straight-bladed VAWT (SB-VAWT) architecture incorporating flexible, scalable auxiliary blades aimed at enhancing both low-speed start-up characteristics and high-speed aerodynamic performance, as shown in Figure 1. The system was designed to integrate a flexible blade connected to a by-blade, actuated by torsional and spiral springs, enabling automatic deployment and retraction as a function of rotor speed. Under low tip speed ratios (TSRs), centrifugal forces were found to be insufficient to overcome the spring tension; therefore, the flexible blade was kept fully deployed, forming a locally drag-dominated rotor configuration that was shown to increase the net moment coefficient (C_M) and to mitigate the poor self-starting capability typical of Darrieus rotors. At higher TSRs, centrifugal forces were shown to exceed the spring stiffness, causing the flexible blade to be retracted into the by-blade, thereby restoring a lift-driven aerodynamic profile and improving aerodynamic energy utilization. CFD simulations were demonstrate that under deployment, the auxiliary module produced a substantial increase in C_M at low TSRs, improving starting torque and rotational acceleration characteristics. Additionally, the system was shown to exhibit improved C_M at moderate-to-high TSRs, indicating that the lift-recovery phase did not compromise high-speed performance and, in specific operating ranges, provided measurable aerodynamic benefits. The performance behavior described in the simulations was observed to align with the operating principle illustrated in Figure 2, where the auxiliary blade was shown to transition between deployed and retracted states depending on angular velocity and associated spring forces. Structural parameters, such as a main blade radius of $R_1 = 0.4$ m, auxiliary radius of $R_2 = 0.25$ m, and inter-blade angle of $\alpha = 60°$, were found to influence the deployment mechanics and torque response (Li et al., 2016). Overall, Li et al. concluded that the flexible, scalable auxiliary blade system addresses two major deficiencies of SB-VAWTs: low-speed self-start and limited aerodynamic efficiency at high TSRs (Li et al., 2016).

Figure 1: Two-dimensional schematic of the proposed SB-VAWT configuration

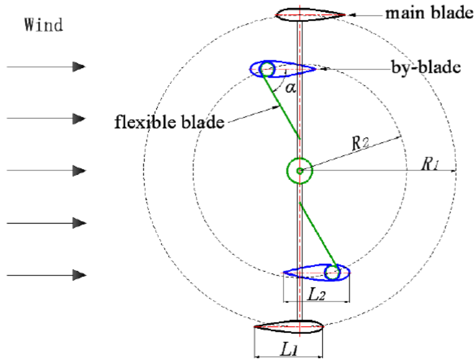

Source: (Li et al., 2016)

Chen et al. (2017) investigated a modified Darrieus rotor featuring two sets of blades mounted in parallel along each radial arm, with varying separation distances (S) between inner (r_{in}) and outer (r_{out}) blade rings, as shown in Figure 2a. Unlike earlier auxiliary blade studies that attempted to enhance VAWT performance through camber augmentation or passive flaps, this configuration was introduced as a dual-ring lift surface concept intended to influence torque generation and power output simultaneously. CFD simulations were reported to reveal that increasing S resulted in a substantial rise in static torque, with maximum improvements reaching approximately 102.1% relative to the baseline configuration, although this was found to come at the cost of a C_P reduction up to 54.4% compared to a traditional single-ring rotor. Azimuthal analysis in Figure 2b demonstrated that while the BB200 configuration exhibited the highest instantaneous power, the traditional Darrieus rotor (TDR) was shown to produce higher positive power output in specific azimuth sectors, particularly 30°–80°, 150°–200°, and 270°–320°, due to more favorable lift development and reduced negative torque. Flow field analysis was found to indicate that larger separation distances enhanced coherent vortex formation and pressure differentials on both blade surfaces, contributing to improved aerodynamic loading at certain rotational positions. Conversely, in static conditions, increasing S was observed to lower the pressure differential between leading and trailing edges due to decreased channel resistance, progressively converging toward TDR-like behavior at sufficiently large spacing. The authors concluded that the dual-blade configuration enhanced starting ability through torque amplification but simultaneously reduced mean power output, implying a trade-off between self-starting performance and energy conversion efficiency (Chen et al., 2017). This approach was therefore stated to differ fundamentally from other auxiliary-blade or add-on devices, which typically aim to achieve simultaneous gains in self-start and C_P, while the dual-ring system was shown to prioritize starting torque at the expense of overall aerodynamic efficiency (Chen et al., 2017).

Figure 2: (a)Top-view configuration of the rotor with dual blade sets; (b) corresponding distribution of instantaneous power output at the optimal TSR

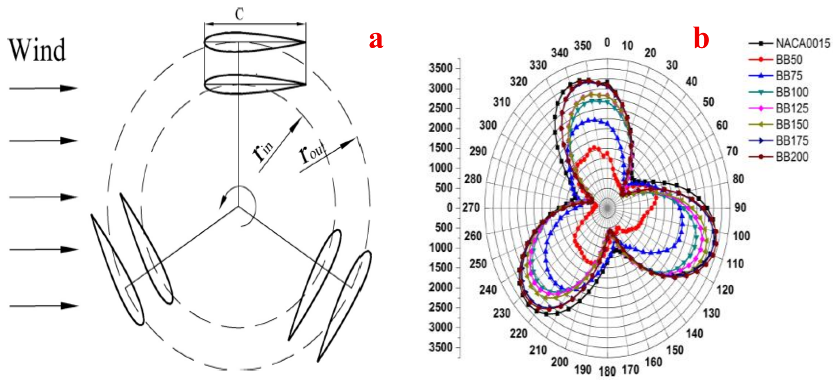

Source: (Chen et al., 2017)

Arpino et al. (2017) investigated a micro-scale Darrieus VAWT employing paired main–auxiliary blades with different chord lengths (C_1, C_2), specifically optimized for low wind speed operation. Using OpenFOAM with a moving mesh approach, multiple turbulence models were compared, and it was demonstrated that the Spalart–Allmaras and SST k–ω models provided the most accurate prediction of the experimental C_P–TSR curves, with Spalart–Allmaras showing the best overall agreement. Experimental wind-tunnel tests confirmed that numerical predictions tended to exceed the measured C_P at TSR > 1.1, whereas torque–azimuth profiles were reproduced with strong agreement by both turbulence models (Arpino et al., 2017). The study emphasized that the moving mesh CFD approach with Spalart–Allmaras offered reliable performance prediction for micro VAWTs employing auxiliary blades, although discrepancies were observed at higher TSR due to increased flow unsteadiness and model sensitivity. Unlike many auxiliary-blade studies focused solely on numerical results, this work was shown to provide direct CFD–experiment correlation on a physical prototype, enhancing its applicability to real small-scale wind harvesting systems (Arpino et al., 2017).

Figure 3: (a) Schematic of the two-bladed micro wind turbine; (b) 3D-printed prototype of the device

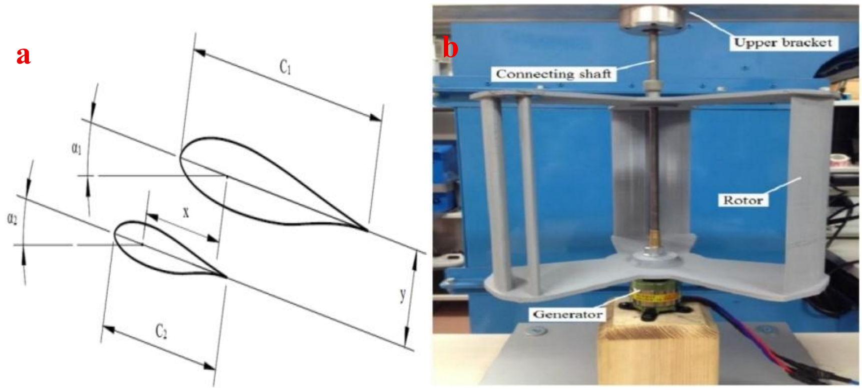

Source: (Arpino et al., 2017)

Wind-tunnel testing by Scungio et al. (2016) on a micro-scale Darrieus rotor employing paired main–auxiliary airfoils with unequal chord lengths was conducted to assess its aerodynamic response under low-TSR conditions. It was demonstrated that the proposed configuration substantially improved low-TSR performance relative to a standard three-bladed baseline. At 6 m/s, C_P =0.082 and C_T =0.098 were attained by the modified rotor, whereas the standard rotor was unable to self-start, thereby indicating a meaningful extension of the operational TSR range (≈0.5–1.2 versus ≈1.0–1.6) (Scungio et al., 2016). Although a slightly higher peak C_P≈0.16 at 14 m/s was recorded for the standard three-blade rotor, higher torque (C_T≈0.153) was produced by the proposed configuration at sub-optimal TSR, resulting in faster acceleration and improved responsiveness to wind fluctuations (Scungio et al., 2016).

Figure 4: C_P and C_T versus TSR: (a) wind-tunnel results at 11 m/s; (b) wind-tunnel results at 15 m/s

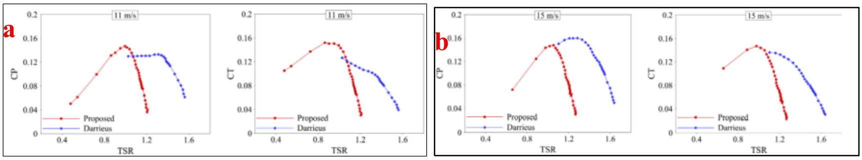

Source: (Scungio et al., 2016)

A real-scale Darrieus VAWT configuration employing three pairs of main–auxiliary airfoils, previously validated at model scale, was analyzed by Arpino et al. (2018) to evaluate its viability for low-wind domestic energy applications. Numerical results indicated that the full-scale rotor attained a maximum $C_P \approx 0.18$ at TSR ≈ 1.5 and a maximum $C_T \approx 0.13$ at TSR ≈ 1.2, significantly outperforming traditional straight-bladed Darrieus rotors at low TSR values. Analysis of azimuthal torque curves revealed that a single main–auxiliary pair generated positive torque between 37° and 160°, with peak torque at ≈100° and a minimum at ≈320°, consistent with vortex-induced lift enhancement mechanisms. Importantly, simulations predicted usable performance even at very low wind speeds (3 m/s), with $C_P \approx 0.10$ and $C_T \approx 0.07$, indicating that the auxiliary-blade architecture enabled energy harvesting in suburban flow conditions whereas conventional Darrieus designs stalled (Arpino et al., 2018). Consequently, unlike previous auxiliary-blade concepts that were primarily tested numerically, full-scale results confirmed that the pairing of main and auxiliary airfoils improved both efficiency and torque at low wind speeds, substantiating its suitability for small-scale, off-grid deployment (Arpino et al., 2018).

Figure 5: (a) Position relationship between the main and auxiliary blades; (b) variation of the average C_{TS} with incoming wind speed

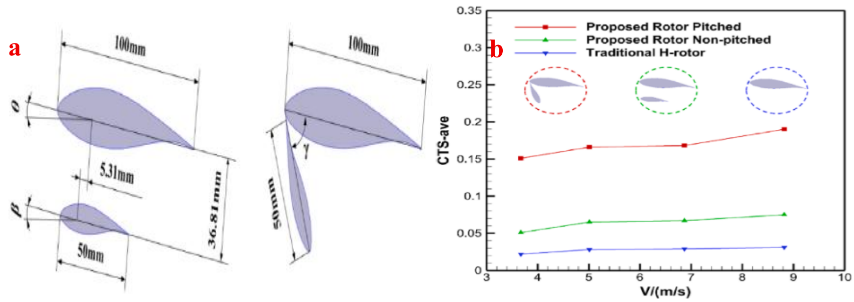

Source: (Su et al., 2020b)

A novel three-pair straight-bladed VAWT featuring a fixed main blade and a rotatable auxiliary blade, whose relative orientation determined the aerodynamic configuration as illustrated in Figure 5, was developed by Su et al. (2020b). Wind-tunnel experiments indicated that all azimuthal static torque coefficients (C_{TS}) of the pitched rotor were positive at the tested wind speeds, demonstrating that self-starting from any azimuthal angle was achievable, in contrast to conventional H-rotors. Quantitatively, substantially higher average C_{TS} values, approximately 3–4 times greater than those of the non-pitched configuration and the traditional H-type rotor, were obtained. Unlike most auxiliary-blade concepts that aimed solely to enhance aerodynamic efficiency through passive camber modification, dynamic pitch ability was incorporated in this design, allowing real-time alteration of flow structures. As a consequence, a higher C_P than that of the H-rotor was exhibited across 4.54–8.82 m/s, with performance improvements concentrated at low rotational speeds due to a shift in optimal TSR. Additionally, pitch control enabled nearly constant power output over varying wind speeds, indicating the presence of an inherent mechanism for aerodynamic load regulation and power smoothing. Therefore, unlike previous auxiliary-blade designs driven by static aerodynamic enhancement, it was demonstrated that active geometric reconfiguration could simultaneously improve self-starting, energy capture, and power controllability in medium-scale VAWTs (Su et al., 2020b).

Figure 6: (a) CAD model of the Double-Darrieus hybrid VAWT showing top, front, and isometric views (dimensions in meters); (b) relative velocity distribution on horizontal iso-planes, including velocity variation along the xz-plane at y = 1.5 m and velocity contours of a single-rotor turbine with an equivalent swept area

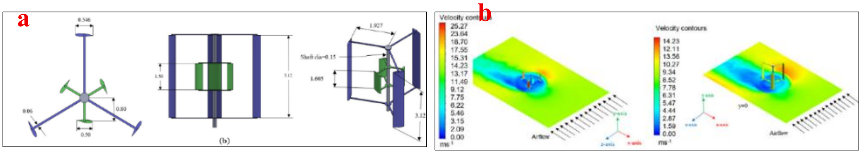

Source: (Ahmad et al., 2022)

A straight-bladed Double-Darrieus hybrid VAWT was proposed by Ahmad et al. (2022) and its geometric parameters were optimized using the Box–Behnken response surface methodology coupled with 3D CFD simulations, as schematically illustrated in Figure 6. The statistically derived optimum configuration (chord length 0.547 m, pitch angle −3.41°, three blades, rotor height 1.605 m, and blade offset 0.789 m) was found to yield a maximum C_P of 0.491 at TSR = 3 and a self-starting cut-in speed of 2.81 m s^{-1}, which was markedly lower than that of conventional H-rotors and existing hybrid VAWTs. The C_{Ts} was observed to remain positive throughout the full azimuthal cycle, confirming complete self-starting capability, while a rated power of 1.522 kW at 7.5 m s^{-1} was achieved, enabling domestic-scale energy production. In comparison with previous auxiliary-blade or hybrid concepts, most of which focused primarily on PFC or qualitative improvements in start-up behavior, quantitative multi-parameter optimization with statistically validated regression models, high R^2 values (~96–98%), and CFD-based cut-in prediction was provided in this study, facilitating early-stage design screening (Ahmad et al., 2022). The results demonstrated that the proposed hybrid topology could simultaneously attain high C_P and low cut-in speed, indicating its potential suitability for small- to mid-scale VAWT deployment under low-wind regimes (Ahmad et al., 2022).

Figure 7: (a) Schematic representation of the Darrieus turbine equipped with auxiliary blades; (b) comparison of the C_P between the standard Darrieus rotor and the auxiliary-blade configuration

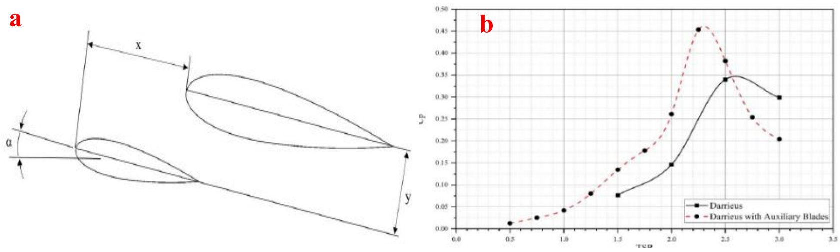

Source: (Asadbeigi et al., 2023)

A CFD-based aerodynamic optimization and economic assessment of a straight-bladed Darrieus VAWT equipped with auxiliary blades was conducted by Asadbeigi et al. (2023) to identify the most efficient and cost-effective configuration for small-scale wind energy applications. SST k–ω simulations coupled with a Kriging surrogate-based optimization framework were employed to evaluate the influence of turbine solidity, chord thickness, aspect ratio, and pitch angle on rotor performance, and an optimal configuration yielding a maximum $C_p = 0.457$at $\lambda = 2.8$ was subsequently derived. A distinct contribution relative to earlier auxiliary-blade studies was provided by the simultaneous integration of aerodynamic optimization and techno-economic evaluation, wherein the optimal Darrieus–auxiliary design, schematically depicted in Figure 7a, was embedded into a hybrid energy system model and was shown to reduce net present cost and levelized cost of energy. The CFD results demonstrated that auxiliary blades enabled power production over a wider TSR interval and that self-starting capability was improved by approximately 75% relative to the baseline Darrieus rotor, while high efficiency at optimal TSR was preserved. Moreover, Figure 7b illustrated that the auxiliary-equipped turbine consistently outperformed the conventional Darrieus rotor across a broad TSR range, confirming the aerodynamic benefit of the adopted auxiliary configuration (Asadbeigi et al., 2023). These findings indicated that the optimized auxiliary-blade turbine could deliver higher aerodynamic efficiency and superior low-speed responsiveness while satisfying economic feasibility criteria in off-grid hybrid energy systems (Asadbeigi et al., 2023).

Figure 8: (a) Blade profiles of auxiliary airfoils; (b) fabricated H-rotor prototypes with auxiliary blades; (c) C_P variation of the auxiliary H-rotor for different AR

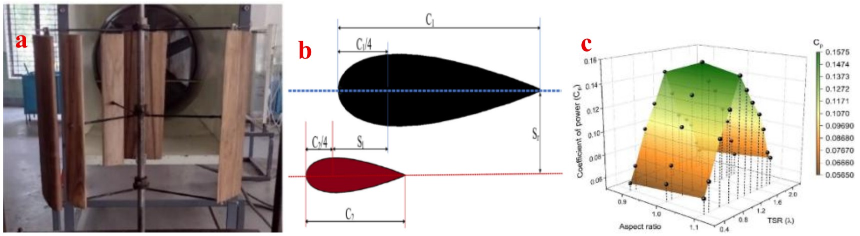

Source: (Reddy et al., 2023)

The influence of AR variation and auxiliary airfoil integration on an H-type Darrieus rotor operating at low wind speeds (4–8 m/s) was experimentally investigated by Reddy et al. (2023) using two fabricated configurations (standard and auxiliary) that were tested in a wind tunnel, as shown in Figure 8. A markedly superior self-starting capability was exhibited by the auxiliary rotor, with a maximum C_{TS} of $C_{ts} = 0.119$, approximately 80.3% higher than that of the standard rotor (0.066), while positive $C_{ts}$was maintained over the entire azimuthal cycle. Dynamic performance was also improved, as the stable TSR operating window was expanded to 0.35–2.2 for the auxiliary configuration compared with 0.4–1.9 for the standard turbine, indicating enhanced robustness under varying inflow conditions. Across all wind speeds and aspect ratios, the maximum C_P of the auxiliary turbine exceeded that of the standard by roughly 4–5%, with the optimal aspect ratio of 1.0 yielding $C_p \approx 0.142$at TSR ≈ 1.10, compared with $C_p \approx 0.136$at TSR ≈ 1.13 for the standard rotor (at 4 m/s). These improvements were attributed to two aerodynamic mechanisms: (i) division of the frontal area, which increased momentum capture, and (ii) suppression of shear-layer reattachment, which enhanced lift-to-drag characteristics on the main blade. Figure 8 presents the blade profiles of the main and auxiliary airfoils, the fabricated rotors, and the variation of $C_p$with aspect ratio for the auxiliary rotor, emphasizing the superior performance of AR = 1.0 (Reddy et al., 2023). Unlike prior auxiliary-blade studies focused on static geometry or dual-blade interactions, the auxiliary blades were systematically coupled with aspect-ratio variation in this work, and it was demonstrated that the height-to-diameter proportion fundamentally governed the efficacy of auxiliary-blade benefits (Reddy et al., 2023).

A multi-blade local variable-radius VAWT intended to enhance self-starting and low-TSR performance in urban wind regimes was investigated by Huang et al. (2023) using four experimentally tested configurations in which the inner blade radius $R_1$was reduced to 0.375–0.625 of the outer radius. Substantial gains in C_{TS} were obtained as $R_1$was reduced; the modified configurations produced C_{Ts} values that were 0.1×, 1.8×, and 2.8× higher than that of the baseline, demonstrating marked improvements in self-starting capability across all azimuthal positions. In terms of power generation, higher $C_p$values than the baseline were achieved by all modified rotors for TSR < 2.2, with maximum benefit at TSR ≈ 2.0, whereas TSR > 2.2 led to blockage effects induced by the inner blades at higher TSRs, reducing energy extraction and degrading C_p. Instantaneous C_{TS} analysis (Figure 9c) showed that the baseline rotor exhibited vortex-induced negative torque beyond 225°, while the reduced-radius configuration maintained positive torque between 250° and 360°, attributed to smoother inflow and attenuation of vortex shedding. The improved low-TSR performance was attributed to dynamic stall mitigation and favorable pressure redistribution on the inner blades at reduced radii, whereas the degraded high-TSR performance was linked to wake blockage scaling with R_1. The tested geometrical arrangement of staggered blade radii was illustrated in Figure 9a, and the comparative power and torque behaviors were summarized in Figure 9b–c, underscoring how local geometric modification reshaped torque production over the azimuth. In contrast to prior auxiliary-blade studies employing secondary airfoils or dual-blade mechanisms, geometric redistribution of blade radii was introduced by Huang et al. (2023) to passively manipulate flow topology without auxiliary surfaces. Overall, the findings indicated that local radius reduction enhanced both self-starting and low-TSR efficiency, making it advantageous for urban or low-wind applications where turbines predominantly operate below optimal TSR (Huang et al., 2023).

Figure 9: (a) Geometry of the local variable-radius VAWT; (b) Comparative variation of C_P *for Model 1-3 over TSR = 1–4; (c) Comparative variation of instantaneous* C_{TS} *of blade A for Model 1 and Model 3 with azimuth angle at TSR = 2*

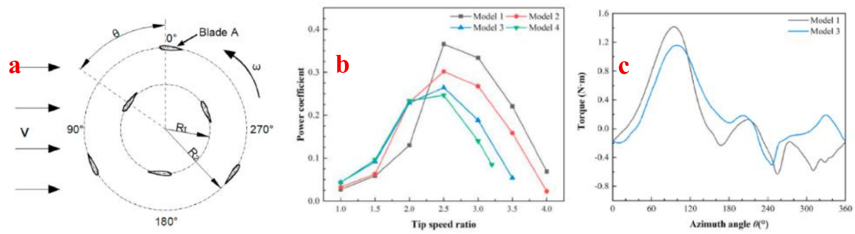

Source: (Huang et al., 2023)

A modified H-type Darrieus rotor equipped with auxiliary blades was numerically and experimentally evaluated by Uma Reddy et al. (2023) with the objective of enhancing self-starting capability and aerodynamic efficiency at low wind speeds. Improvements were obtained for the modified configuration, which achieved $C_{ts} = 0.11$and $C_p = 0.18$, corresponding to 84% and 22% increases over the conventional rotor, respectively. The operational TSR window was expanded from 0.56–1.70 to 0.50–1.98, indicating improved robustness under unsteady inflow. The underlying aerodynamic mechanisms were identified through synchronized flow-field diagnostics. As shown in Figure 10 (a–b), the static pressure distribution around blade 1 at 30° azimuth demonstrated that the auxiliary blades generated substantially greater suction-side loading; the static pressure ranged from −32.3 to 38.2 Pa in the conventional rotor and from −92.2 to 66.8 Pa in the modified rotor. This redistribution of pressure revealed a stronger adverse-pressure-gradient mitigation effect and increased aerodynamic loading. In addition, Figure 10(c) presented azimuth-dependent pressure contours for both rotors, illustrating that the modified configuration reorganized the pressure field during the advancing and returning phases, leading to enhanced momentum recovery and reduced stall severity. Furthermore, Figure 10(d) showed that the auxiliary blades suppressed large-scale vortex shedding and promoted shear-layer reattachment, producing more coherent and attached streamline patterns over the rotor. Collectively, these observations confirmed that the auxiliary blades acted as a boundary-layer flow control device that induced shear-layer reattachment, suppressed turbulence, increased suction-side loading, and strengthened torque production mechanisms, thereby improving power capture in low-wind regimes. While most prior studies focused on geometric variations, solidity effects, or radial offsets, the integration of auxiliary blades with synchronized pressure-field and streamline diagnostics in Uma Reddy et al. (2023) enabled explicit resolution of the phase-dependent flow topology over an entire revolution. Consequently, the study not only demonstrated increases in $C_p$and C_{ts} but also revealed, at a mechanistic level, how auxiliary blades reorganized the time-dependent unsteady vortex dynamics (Uma Reddy et al., 2023).

Figure 10: (a–b) Static pressure distribution around blade 1 at 30° azimuth for both rotor configurations, illustrating the near-blade pressure loading: (a) conventional H-rotor, (b) modified H-rotor (c) Pressure contours as a function of blade position for both rotors, (d) Streamlines over the rotor blades for the two configurations

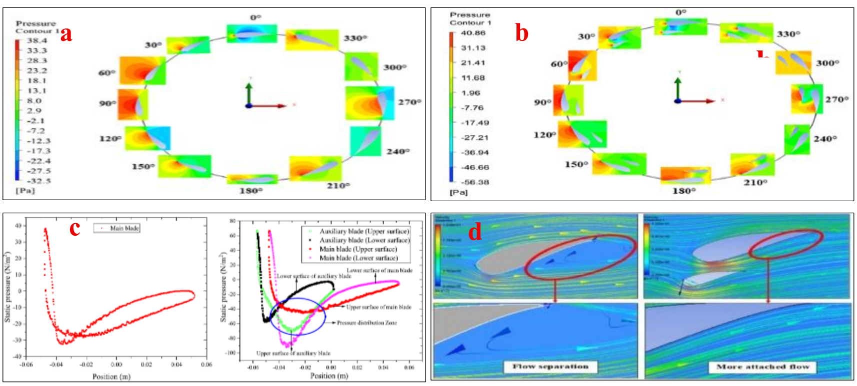

Source: (Uma Reddy et al., 2023)

An NREL S823 airfoil with and without an auxiliary airfoil was experimentally and numerically analyzed by Reddy et al. (2024), and it was demonstrated that the modified configuration

(S823(A)) consistently attained higher lift coefficients, with 10–14% improvements in $C_L$and C_L/C_Dmetrics across low Reynolds-number conditions. Stall delay of approximately 1°–3° was induced by the auxiliary airfoil, abrupt drag escalation was suppressed, and post-stall aerodynamics were stabilized through more controlled separation dynamics (Uma Reddy et al., 2024). Flow-field diagnostics revealed that the S823(A) model exhibited lower suction-side pressure minima and reduced TKE intensity, indicating mitigated vortex shedding and enhanced reattachment behavior (Reddy et al., 2024).

Figure 11: (a) Schematic of the Darrieus VAWT equipped with auxiliary blades and double deflectors; (b) C_P comparison illustrating the effect of deflector installation on turbine performance

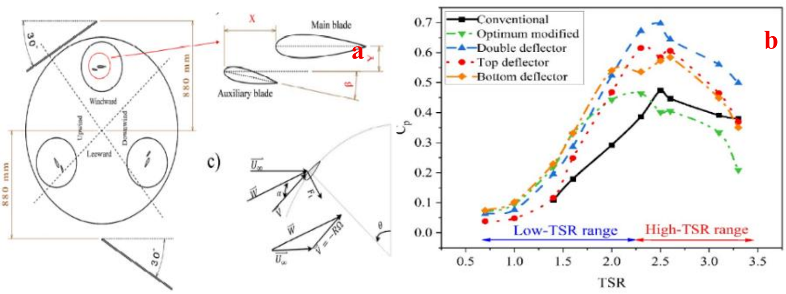

Source: (Ghafoorian et al., 2024)

A CFD-based parametric optimization of a medium-scale Darrieus VAWT (diameter ≈ 1 m) equipped with a single auxiliary blade was performed by Ghafoorian et al. (2024) and the aerodynamic response of the system under multiple deflector configurations was subsequently evaluated. The auxiliary-blade parameters, pitch angle, horizontal spacing (X/C), and vertical spacing (Y/C), were exhaustively screened to enhance self-starting capability without introducing performance penalties at high TSR. The optimized configuration (β = 0°, X/C = 0.52, Y/C = 0.41) was shown to reduce the onset of rotation from TSR ≈ 1.4 to 0.7 and to yield a 59% increase in $C_p$at TSR = 1.4 relative to the baseline rotor, as verified through pressure-field diagnostics (Figure 11b). High-TSR operation of the auxiliary-blade rotor, however, remained penalized due to pronounced flow separation and swirl formation in the downwind sector. To mitigate these losses, passive deflectors—top, bottom, and double—were introduced upstream of the rotor, as schematically depicted in Figure 11(a). Performance-map analysis demonstrated that double deflectors enabled substantial high-TSR performance recovery; $C_p \approx 0.69$at TSR = 2.5 was achieved, representing a 47% improvement over the control rotor ($C_p \approx 0.47$) and a 73% improvement relative to the auxiliary-blade-only configuration ($C_p \approx 0.40$), as illustrated in Figure 11(b). Conversely, the top deflector induced severe low-TSR degradation, decreasing $C_p$by 71% at TSR = 1.4 relative to the bottom-deflector case, while the single bottom deflector produced only modest gains across both regimes. Relative to previous auxiliary-blade studies, including static dual-airfoil additions, fixed secondary blades aimed at torque enhancement, or separation-suppression geometries, the work of Ghafoorian et al. (2024) provided the simultaneous demonstration of (i) auxiliary-blade-driven low-TSR self-starting enhancement and (ii) deflector-mediated high-TSR efficiency recovery within a unified PFC framework. Whereas earlier studies typically reported improved low-TSR torque at the expense of peak power due to blade-to-blade interference, the staged PFC strategy validated here supplied bidirectional operating-range enhancement: stall mitigation and torque amplification at low TSR via auxiliary blades, followed by wake-channeling and re-energization at high TSR via double deflectors (Ghafoorian et al., 2024).

Figure 12: Instantaneous streamline structures and normalized velocity fields for rotors configured with attachment angles of 0°, 15° and 30° and evaluated at an azimuth position of 0° under operating conditions of TSR = 1.5 and incoming wind speed U = 10 m/s

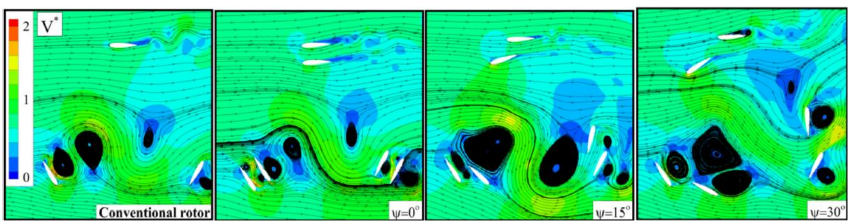

Source: (Mohammadnejad & Hassanzadeh, 2025).

A 2D URANS-based CFD investigation of a three-bladed Darrieus VAWT equipped with auxiliary blades was conducted by Mohammadnejad and Hassanzadeh (2025) examining attachment angles $\psi = 0°, 15°$and $30°$under free-stream velocities of 7–14 m/s and TSR = 0.5–2.5. The configuration with $\psi = 0°$was found to offer the highest performance, attaining mean C_P values of 0.2713, 0.3265, and 0.3607 at $U = 7,10,$and 14 m/s, corresponding to increases of 7.02%, 18.72%, and 18.26% over the baseline rotor. The underlying flow mechanisms were identified through instantaneous streamline and normalized-velocity diagnostics, as shown in Figure 12, where the rotor was evaluated at an azimuth position of 0° under TSR = 1.5 and $U = 10$ m/s. At $\psi = 0°$, large-scale vortical structures originating from the trailing edge of the second main blade were suppressed, and a jet-like flow formed between the main and auxiliary blades, which mitigated separation, stabilized the velocity field, and limited dead-band extension. In contrast, attachment angles $\psi \geq 15°$intensified multi-site separation, promoted vortex coalescence, and deflected incoming flow, producing strong core-flow attenuation and elevated drag on downstream blades. Unlike prior auxiliary-blade studies that emphasized enhanced self-starting or steady-state $C_p$improvements through geometric modification, this work demonstrated that auxiliary-blade performance is highly sensitive to angular positioning and that improper placement can deteriorate rotor performance despite the presence of added lifting surfaces (Mohammadnejad & Hassanzadeh, 2025). Overall, the results established $\psi = 0°$as the most effective PFC configuration, particularly at higher wind speeds and mid-TSR regimes, while revealing severe degradation when auxiliary blades disturbed intra-rotor flow topology (Mohammadnejad & Hassanzadeh, 2025).

A two-dimensional CFD and wind-tunnel investigation was conducted by Reddy et al. (2025) to evaluate an H-type Darrieus rotor equipped with auxiliary airfoils across aspect ratios of 0.9–1.1 and wind speeds of 4–8 m/s. It was demonstrated that auxiliary-blade integration markedly increased self-starting torque, expanded the operational TSR envelope, and enhanced power output relative to the standard configuration. Flow-field diagnostics further revealed the aerodynamic mechanisms responsible for these improvements. As shown in Figure 13 (a–b), the standard rotor exhibited intense circular streamline formation over blade 1 at 30° azimuth, generating elevated pressure drag, whereas the auxiliary-blade rotor suppressed vortex recirculation and promoted shear-layer reattachment, resulting in enhanced lift production and reduced drag. Unlike earlier auxiliary-blade studies that primarily examined static geometric modifications or isolated chord-length effects, Reddy et al. demonstrated a synergistic dependence on aspect ratio, identifying AR = 1.0 as the optimum configuration for maximizing torque and minimizing stall-induced losses (Reddy et al., 2025). Additionally, the study showed that auxiliary blades not only acted as passive boundary-layer control devices but also reorganized internal rotor aerodynamics by modifying separation loci and enabling post-stall performance recovery, an outcome not commonly achieved in small-scale VAWT augmentation studies (Reddy et al., 2025).

Figure 13: Streamline topology over the tested rotors at an azimuth angle of 30°: (a) conventional H-rotor; (b) auxiliary-blade-equipped H-rotor

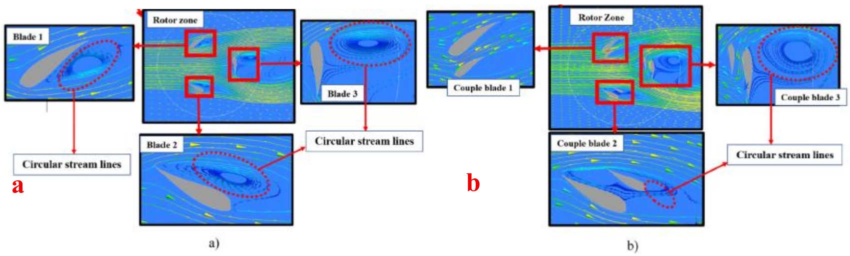

Source: (Reddy et al., 2025).

Experimental testing by Kumara and Yoga (2025) on a two-bladed hybrid Darrieus–Savonius rotor equipped with auxiliary NACA 4418 blades and variable overlap ratios demonstrated that hybridization can substantially enhance low-speed starting torque and aerodynamic efficiency relative to a standalone Darrieus configuration. The optimal configuration, achieved with an overlap ratio of −0.5 and auxiliary-blade spacing of 17 cm, delivered the highest $C_p = 0.018$ at TSR ≈ 0.78 and 5 m/s, while increasing the C_{Ts} to 0.045 at 3 m/s and 0°, confirming improved initial self-starting characteristics (Y. Kumar & Roga, 2025). Unlike earlier hybrid Darrieus–Savonius studies that focused primarily on torque augmentation via rotor-shape interactions, this work establishes that auxiliary Darrieus blades act as low-Reynolds-number flow-conditioning elements whose optimal axial placement controls both aerodynamic loading and operational TSR bandwidth (Y. Kumar & Roga, 2025).

Conclusion

Across the reviewed literature, auxiliary-blade integration has emerged as a versatile PFC strategy that can systematically improve the aerodynamic behavior of straight-bladed and Darrieus-type VAWTs under low Reynold-number operating conditions. The reviewed studies consistently show that auxiliary blades enhance self-starting capability, expand the stable TSR window, and increase low-TSR torque production, either through drag-dominanted augmentation at low TSR (Y. Kumar & Roga, 2025; Li et al., 2016; Reddy et al., 2025; Scungio et al., 2016) or via controlled lift-enhancement mechanisms that stabilize unsteady flow separation and promote shear-layer reattachment (Uma Reddy et al., 2023, 2024). These benefits are particularly pronounced in configurations optimized for small-scale or urban wind environments, where reduced cut-in speed, rapid acceleration, and responsiveness to fluctuating inflow are dominant performance metrics.

However, multiple investigations also reveal performance penalties at high TSR, including reduced peak C_{Ps}, increased drag, and flow blockage, particularly when auxiliary elements introduce persistent wake interference or amplify downwind separation (Chen et al., 2017; Ghafoorian et al., 2024; Huang et al., 2023). To address this aerodynamic trade-off, recent studies propose adaptive or staged hybrid strategies, such as flexible auxiliary blades that retract under centrifugal loading to restore lift-driven operation (Li et al., 2016) or deflectors to re-energize wakes and recover high-TSR efficiency (Ghafoorian et al., 2024). These approaches suggest that auxiliary-blade functionality is most effective when embedded in a TSR-dependent operational architecture, rather than as a static geometric addition.

The aerodynamic value of auxiliary blades is shown to be highly configuration-dependent, influenced by radial positioning (Y.

Kumar & Roga, 2025), inter-blade spacing (Chen et al., 2017), local radius redistribution (Huang et al., 2023), and relative orientation angle (Mohammadnejad & Hassanzadeh, 2025). This highlights that performance gains arise not only from added lifting surfaces but from deliberate manipulation of intra-rotor flow topology, targeting stall mitigation, vortex suppression, and pressure redistribution over the azimuthal cycle. Nevertheless, the resulting design complexity, increased solidity, and manufacturing costs are non-negligible disadvantages, particularly for small-scale systems where structural simplicity and economic feasibility are crucial. Collectively, the reviewed studies demonstrate that auxiliary-blade concepts can transform traditional Darrieus rotors from high-TSR, lift-only machines into multi-regime and responsive aerodynamic systems capable of enhanced performance in low and moderate wind environments. Yet they also underscore a persistent efficiency–robustness trade-off in low-TSR operation, where improvements in self-starting torque and low-TSR performance may deteriorate peak C_P unless augmented with adaptive mechanisms or complementary passive devices. Future development therefore depends on integrated optimization frameworks that simultaneously account for aerodynamic performance, operational range, manufacturability, and economic viability.

References

Abdel-razak, M. H., Emam, M., Ookawara, S., & Hassan, H. (2026). Study the performance of a novel design of twin hybrid Darrieus-Savonius vertical-axis wind turbines integrated with building water storage tanks: 3D optimization study. *Renewable Energy*, *256*, 124024. https://doi.org/10.1016/J.RENENE.2025.124024

Acir, A., Canli, M. E., Ata, I., Uzun, S., & Tanürün, H. E. (2021). Experimental investigation of thermal energy storage efficiency using fin application with phase change material (PCM) under solar radiation. *Heat Transfer Research*, *52*(6), 21–39. https://doi.org/10.1615/HEATTRANSRES.2021036643

Acır, A., Canlı, M. E., Ata, İ., & Tanürün, H. E. (2019). Effects of a circular-shaped turbulator having varying hole numbers on energy and exergy efficiencies of a solar air heater. *International Journal of Ambient Energy*, *40*(7), 739–748. https://doi.org/10.1080/01430750.2017.1423385

Acır, A., & Tanürün, H. E. (2019). Bir Termik Santralde Isıl Tersinmezliklerin Enerji Verimliliğine Etkisinin İncelenmesi. In M. C. Bağdatlı (Ed.), *2. International Conferance on Energy Research (ENRES)* (pp. 126–132). Enres.

Ahmad, M., Shahzad, A., Akram, F., Ahmad, F., & Shah, S. I. A. (2022). Design optimization of Double-Darrieus hybrid vertical axis wind turbine. *Ocean Engineering*, *254*, 111171. https://doi.org/10.1016/J.OCEANENG.2022.111171

Alanis Ruiz, C., Kalkman, I., & Blocken, B. (2021). Aerodynamic design optimization of ducted openings through high-rise buildings for wind energy harvesting. *Building and Environment*, *202*, 108028. https://doi.org/10.1016/J.BUILDENV.2021.108028

Al-Hadhrami, L. M. (2014). Performance evaluation of small wind turbines for off grid applications in Saudi Arabia. *Energy Conversion and Management*, *81*, 19–29. https://doi.org/10.1016/J.ENCONMAN.2014.01.064

Arpino, F., Cortellessa, G., Dell'Isola, M., Scungio, M., Focanti, V., Profili, M., & Rotondi, M. (2017). CFD simulations of power coefficients for an innovative Darrieus style vertical axis wind turbine with auxiliary straight blades. *Journal of Physics: Conference Series*, *923*(1), 012036. https://doi.org/10.1088/1742-6596/923/1/012036

Arpino, F., Scungio, M., & Cortellessa, G. (2018). Numerical performance assessment of an innovative Darrieus-style vertical axis wind turbine with auxiliary straight blades. *Energy Conversion and Management*, *171*, 769–777. https://doi.org/10.1016/J.ENCONMAN.2018.06.028

Asadbeigi, M., Ghafoorian, F., Mehrpooya, M., Chegini, S., & Jarrahian, A. (2023). A 3D Study of the Darrieus Wind Turbine with Auxiliary Blades and Economic Analysis Based on an Optimal Design from a Parametric Investigation. *Sustainability 2023, Vol. 15, Page 4684*, *15*(5), 4684. https://doi.org/10.3390/SU15054684

Asif, M., & Muneer, T. (2007). Energy supply, its demand and security issues for developed and emerging economies. *Renewable and Sustainable Energy Reviews*, *11*(7), 1388–1413. https://doi.org/10.1016/J.RSER.2005.12.004

Ata, İ., Tanürün, H. E., Uzun, S., Bayrak, S., & Acır, A. (2022). Exergy analysis and determination of irreversibilty of a thermal power plant. *Heat Transfer Research*, *53*(2), 1–12. https://doi.org/10.1615/HEATTRANSRES.2021039997

Azadani, L. N. (2023). Vertical axis wind turbines in cluster configurations. *Ocean Engineering*, *272*, 113855. https://doi.org/10.1016/J.OCEANENG.2023.113855

Aziz, M. A., Gaheen, O. A., Benini, E., & Elsayed, A. M. (2024). Experimental investigation of multi-step airfoils in low Reynolds numbers applications. *Heliyon*, *10*(12), e32919. https://doi.org/10.1016/J.HELIYON.2024.E32919

Benmoussa, A., & Páscoa, J. C. (2023). Enhancement of a cycloidal self-pitch vertical axis wind turbine performance through DBD plasma actuators at low tip speed ratio. *International Journal of Thermofluids*, *17*, 100258. https://doi.org/10.1016/J.IJFT.2022.100258

Bhuyan, S., & Biswas, A. (2014). Investigations on self-starting and performance characteristics of simple H and hybrid H-Savonius vertical axis wind rotors. *Energy Conversion and Management*, *87*, 859–867. https://doi.org/10.1016/J.ENCONMAN.2014.07.056

Bianchini, A., Balduzzi, F., Rainbird, J. M., Peiró, J., Graham, J. M. R., Ferrara, G., & Ferrari, L. (2015). On the influence of virtual camber effect on airfoil polars for use in simulations of Darrieus wind turbines. *Energy Conversion and Management*, *106*, 373–384. https://doi.org/10.1016/J.ENCONMAN.2015.09.053

Çakıroğlu, R., Tanürün, H. E., Acır, A., Üçgül, F., & Olkun, S. (2023). Optimization of NACA 4412 augmented with a gurney flap by using grey relational analysis. *Journal of the Brazilian Society of Mechanical Sciences and Engineering 2023 45:3*, *45*(3), 167-. https://doi.org/10.1007/S40430-023-04089-X

Chen, J., Liu, P., Xu, H., Chen, L., Yang, M., & Yang, L. (2017). A detailed investigation of a novel vertical axis Darrieus wind rotor with two sets of blades. *Journal of Renewable and Sustainable Energy*, *9*(1). https://doi.org/10.1063/1.4977004/285300

Davari, H. S., Botez, R. M., Davari, M. S., & Chowdhury, H. (2024). Enhancing the Efficiency of Horizontal Axis Wind Turbines Through Optimization of Blade Parameters. *Journal of Engineering*, *2024*(1), 8574868. https://doi.org/10.1155/2024/8574868

Exner, A., Politti, E., Schriefl, E., Erker, S., Stangl, R., Baud, S., Warmuth, H., Matzenberger, J., Kranzl, L., Paulesich, R., Windhaber, M., Supper, S., & Stoeglehner, G. (2016). Measuring regional resilience towards fossil fuel supply constraints. Adaptability and vulnerability in socio-ecological Transformations-the case of Austria. *Energy Policy*, *91*, 128–137. https://doi.org/10.1016/J.ENPOL.2015.12.031

Fadaei, M., Davari, A. R., Sabetghadam, F., & Soltani, M. R. (2021). Enhancement of a horizontal axis wind turbine airfoil performance using single dielectric barrier discharge plasma actuator. *Proceedings of the Institution of Mechanical Engineers, Part A: Journal of Power and Energy*, *235*(3), 476–493. https://doi.org/10.1177/0957650920936026.

Fouatih, O. M., Medale, M., Imine, O., & Imine, B. (2016). Design optimization of the aerodynamic passive flow control on NACA 4415 airfoil using vortex generators. *European Journal of Mechanics - B/Fluids*, *56*, 82–96. https://doi.org/10.1016/J.EUROMECHFLU.2015.11.006

Gad-el-Hak, M. (2012). Flow Control: The Future. *Https://Doi.Org/10.2514/2.2796*, *38*(3), 402–418. https://doi.org/10.2514/2.2796

Ghafoorian, F., Enayati, E., Mirmotahari, S. R., & Wan, H. (2024). Self-Starting Improvement and Performance Enhancement in Darrieus VAWTs Using Auxiliary Blades and Deflectors. *Machines 2024, Vol. 12, Page 806*, *12*(11), 806. https://doi.org/10.3390/MACHINES12110806

Ghafoorian, F., Mirmotahari, S. R., Eydizadeh, M., & Mehrpooya, M. (2025). A systematic investigation on the hybrid Darrieus-Savonius vertical axis wind turbine aerodynamic performance and self-starting capability improvement by installing a curtain. *Next Energy*, *6*, 100203. https://doi.org/10.1016/J.NXENER.2024.100203

Guo, J., Zeng, P., & Lei, L. (2019). Performance of a straight-bladed vertical axis wind turbine with inclined pitch axes by wind tunnel experiments. *Energy*, *174*, 553–561. https://doi.org/10.1016/J.ENERGY.2019.02.177

Hao, W., Bashir, M., Li, C., & Sun, C. (2021). Flow control for high-solidity vertical axis wind turbine based on adaptive flap. *Energy Conversion and Management*, *249*, 114845. https://doi.org/10.1016/j.enconman.2021.114845

Hoseinzadeh, S., Astiaso Garcia, D., & Huang, L. (2023). Grid-connected renewable energy systems flexibility in Norway islands' Decarbonization. *Renewable and Sustainable Energy Reviews*, *185*, 113658. https://doi.org/10.1016/J.RSER.2023.113658

Huang, H., Li, J., & Li, G. (2023). Improving the self-starting and operating characteristics of vertical axis wind turbine by changing center distance in part of blades. *Journal of Building Engineering*, *68*, 105974. https://doi.org/10.1016/J.JOBE.2023.105974

Ibrahim, A. A., Elbaz, A. M. R., Melani, P. F., Mohamed, O. S., & Bianchini, A. (2022). Power augmentation of Darrieus wind turbine blades using trapped vortex cavity. *Journal of Wind Engineering and Industrial Aerodynamics*, *223*. https://doi.org/10.1016/j.jweia.2022.104949

Kabeyi, M. J. B., & Olanrewaju, O. A. (2022). Sustainable Energy Transition for Renewable and Low Carbon Grid Electricity Generation and Supply. *Frontiers in Energy Research*, *9*, 743114. https://doi.org/10.3389/FENRG.2021.743114/FULL

Kaya, A. F., Tanürün, H. E., & Acir, A. (2022). Numerical Investigation of Radius Dependent Solidity Effect on H-Type Vertical Axis Wind Turbines. *Journal of Polytechnic*, *25*(3), 1007–1019. https://doi.org/10.2339/POLITEKNIK.799767

Ke, W., Hashem, I., Zhang, W., & Zhu, B. (2022). Influence of leading-edge tubercles on the aerodynamic performance of a horizontal-axis wind turbine: A numerical study. *Energy*, *239*. https://doi.org/10.1016/j.energy.2021.122186

Koşan, M., Tanürün, H. E., & Martin, K. (2024). Yeşil Teknolojiler ve Enerji: Rüzgar, Güneş, Biyogaz. In M. Koşan (Ed.), *Yeşil Teknolojiler ve Enerji: Rüzgar, Güneş, Biyogaz* (1st ed., Vol. 1, Issue 1). Bidge Yayınları. https://doi.org/10.70269/N6THV48NSN99

Kumar, S., & Rathore, K. (2023). Renewable Energy for Sustainable Development Goal of Clean and Affordable Energy. *International Journal of Materials Manufacturing and Sustainable Technologies*, *2*(1), 1–15. https://doi.org/10.56896/IJMMST.2023.2.1.001

Kumar, Y., & Roga, S. (2025). Design and Performance Analysis of Hybrid VAWTs with Varying Auxiliary Blade Symmetry and Overlap Ratios: An Experimental Study. *Fluid Dynamics 2025 60:4*, *60*(4), 85-. https://doi.org/10.1134/S0015462825600798

Kutluca, T. O., Koç, E., & Yavuz, T. (2023). Synthetic jet application in the wind turbine concentrator design. *Energy Sources, Part A: Recovery, Utilization and Environmental Effects*, *45*(2), 5789–5805. https://doi.org/10.1080/15567036.2023.2208072;ISSUE:ISSUE:DOI

Li, Y., Wang, H., & Wu, Z. (2022). Aerodynamic characteristic of wind turbine with the leading edge slat and Microtab. *Sustainable Energy Technologies and Assessments*, *52*, 101957. https://doi.org/10.1016/J.SETA.2022.101957

Li, Y., Zhao, C., Qu, C., Zhao, S., Feng, F., & Tagawa, K. (2019). Effect of Auxiliary Blade on Aerodynamic Characteristics of Vertical Axis Wind Turbine by Numerical Simulation. *International Journal of Rotating Machinery*, *2019*. https://doi.org/10.1155/2019/8098160

Li, Y., Zhao, S., Tagawa, K., & Feng, F. (2018). Starting performance effect of a truncated-cone-shaped wind gathering device on small-scale straight-bladed vertical axis wind turbine. *Energy Conversion and Management*, *167*, 70–80. https://doi.org/10.1016/J.ENCONMAN.2018.04.062

Li, Y., Zheng, Y. F., Feng, F., He, Q. B., & Wang, N. X. (2016). Numerical simulation on a straight-bladed vertical axis wind turbine with auxiliary blade. *IOP Conference Series: Earth and Environmental Science*, *40*(1), 012062. https://doi.org/10.1088/1755-1315/40/1/012062

Liu, J., Lin, H., & Zhang, J. (2019). Review on the technical perspectives and commercial viability of vertical axis wind turbines. *Ocean Engineering*, *182*, 608–626. https://doi.org/10.1016/J.OCEANENG.2019.04.086

Matiz-Chicacausa, A., Molano, S., & Lopez Mejia, O. D. (2023). Flow Control with Synthetic Jets on a Wind Turbine Airfoil. *AIAA Aviation and Aeronautics Forum and Exposition, AIAA AVIATION Forum 2023*. https://doi.org/10.2514/6.2023-3526

McCollum, D., Bauer, N., Calvin, K., Kitous, A., Riahi, K., Weyant, J., Kriegler, E., Blanford, G., Krey, V., Edmonds, J., Richels, R., Tavoni, M., McCollum, D., Riahi, K., Bauer, N., Calvin, K., & Kitous, A. (2013). Fossil resource and energy security dynamics in conventional and carbon-constrained worlds. *Climatic Change 2013 123:3*, *123*(3), 413–426. https://doi.org/10.1007/S10584-013-0939-5

Mirmotahari, S. R., Ghafoorian, F., & Zanj, A. (2025). Parametric study on self-starting capability and aerodynamic performance of a hybrid J-shaped Darrieus vertical axis wind turbine. *Physics of Fluids*, *37*(11), 115122. https://doi.org/10.1063/5.0296660/3371520

Mishriky, F., & Walsh, P. (2016). Effect of the Backward-Facing Step Location on the Aerodynamics of a Morphing Wing. *Aerospace 2016, Vol. 3, Page 25*, *3*(3), 25. https://doi.org/10.3390/AEROSPACE3030025

Mohammadnejad, M., & Hassanzadeh, R. (2025). Impacts of Auxiliary Blades on the Performance of a Three-Bladed Darrieus Wind Turbine. *Arabian Journal for Science and Engineering 2025*, 1–18. https://doi.org/10.1007/S13369-025-10542-X

Paraschivoiu, I. (2009). *Wind Turbine Design: With Emphasis on Darrieus Concept - Ion Paraschivoiu - Google Kitaplar* (S. Schettini, Ed.).

Reddy, K. U., Deb, B., & Roy, B. (2023). Experimental Study on Influence of Aspect Ratio and Auxiliary Blade Profile on the Performance of H-Type Darrieus Wind Rotor. *Arabian Journal for Science and Engineering 2023 49:2*, *49*(2), 1913–1929. https://doi.org/10.1007/S13369-023-08049-4

Reddy, K. U., Deb, B., & Roy, B. (2025). Innovative Strategy for Enhancing Performance in H-Type Darrieus Wind Turbines. *Arabian Journal for Science and Engineering 2025*, 1–23. https://doi.org/10.1007/S13369-025-10435-Z

Rezaeiha, A., Kalkman, I., & Blocken, B. (2017). Effect of pitch angle on power performance and aerodynamics of a vertical axis wind turbine. *Applied Energy*, *197*, 132–150. https://doi.org/10.1016/j.apenergy.2017.03.128

Rezaeiha, A., Montazeri, H., & Blocken, B. (2018). Characterization of aerodynamic performance of vertical axis wind turbines: Impact of operational parameters. *Energy Conversion and Management*, *169*, 45–77. https://doi.org/10.1016/J.ENCONMAN.2018.05.042

Salman, M., Tanürün, H. E., Acır, A., & Kaya, A. F. (2019). NACA 4412 kanat modeli yapisinda çukur etkisinin sayisal analizi. In M. C. Bağdatlı (Ed.), *2. International Conferance on Energy Research (ENRES)* (p. 133).

Scungio, M., Arpino, F., Focanti, V., Profili, M., & Rotondi, M. (2016). Wind tunnel testing of scaled models of a newly developed Darrieus-style vertical axis wind turbine with auxiliary straight blades. *Energy Conversion and Management*, *130*, 60–70. https://doi.org/10.1016/J.ENCONMAN.2016.10.033

Seifi Davari, H., Botez, R. M., Seify Davari, M., Chowdhury, H., & Hosseinzadeh, H. (2024a). Blade height impact on self-starting torque for Darrieus vertical axis wind turbines. *Energy Conversion and Management: X*, *24*, 100814. https://doi.org/10.1016/J.ECMX.2024.100814

Seifi Davari, H., Botez, R. M., Seify Davari, M., Chowdhury, H., & Hosseinzadeh, H. (2024b). Numerical and experimental investigation of Darrieus vertical axis wind turbines to enhance self-starting at low wind speeds. *Results in Engineering*, *24*, 103240. https://doi.org/10.1016/J.RINENG.2024.103240

Seifi Davari, H., Kouravand, S., Seify Davari, M., & Kamalnejad, Z. (2023). Numerical investigation and aerodynamic simulation of Darrieus H-rotor wind turbine at low Reynolds numbers. *Energy Sources, Part A: Recovery, Utilization, and Environmental Effects*, *45*(3), 6813–6833. https://doi.org/10.1080/15567036.2023.2213670

Seifi Davari, H., Mihaela Botez, R., Seify Davari, M., & Chowdhury, H. (2024). Enhancing aerodynamic efficiency: shape modification of airfoils. *International Journal of Ambient Energy*, *45*(1), 2439441. https://doi.org/10.1080/01430750.2024.2439441

Seifi Davari, H., Seify Davari, M., Botez, R. M., & Chowdhury, H. (2025). Advancements in Vertical Axis Wind Turbine Technologies: A Comprehensive Review. *Arabian Journal for Science and Engineering*, *50*(4), 2169–2216. https://doi.org/10.1007/S13369-024-09723-X

Seifi Davari, H., Seify Davari, M., & Ntantis, E. L. (2025). A review on the design and optimization of lift-based hydrokinetic turbines: Darrieus, Gorlov, and helical types. *Results in Engineering*, *28*, 107746. https://doi.org/10.1016/J.RINENG.2025.107746

Seyhan, M., & Tanürün, H. E. (2024). Experimental optimization of the SG6043 airfoil for horizontal axis wind turbine using Schmitz equations. *International Journal of Energy Studies*, *9*(4), 619–636. https://doi.org/10.58559/IJES.1552364

Seyhan, M., Tanürün, H. E., Aydin, N., & Ayyildiz, E. (2025). Strategic site selection for biohydrogen production: Enhancing rural sustainability through agricultural biomass. *Energy for Sustainable Development*, *89*, 101838. https://doi.org/10.1016/J.ESD.2025.101838

Su, H., Dou, B., Qu, T., Zeng, P., & Lei, L. (2020a). Experimental investigation of a novel vertical axis wind turbine with pitching and self-starting function. *Energy Conversion and Management*, *217*(January), 113012. https://doi.org/10.1016/j.enconman.2020.113012

Su, H., Dou, B., Qu, T., Zeng, P., & Lei, L. (2020b). Experimental investigation of a novel vertical axis wind turbine with pitching and self-starting function. *Energy Conversion and Management*, *217*, 113012. https://doi.org/10.1016/J.ENCONMAN.2020.113012

Sun, Y., Qian, Y., Wang, T., Wang, L., Zhu, C., & Gao, Y. (2024). Investigation of the wind turbine aerodynamic performance via the combining blowing and suction flow control. *Energy*, *307*, 132505. https://doi.org/10.1016/J.ENERGY.2024.132505

Tanürün, H. E. (2023a). Dikey eksenli rüzgâr türbinlerinde kanal teknolojisinin performans üzerine etkisinin kapsamli derlemesi . In N. Akhmetov (Ed.), *IV. Baskent Internatıonal Conference on Multıdıscıplınary Studıes* (pp. 1254–1262). İzdaş.

Tanürün, H. E. (2023b). H-Darrieus Dikey Eksenli Rüzgâr Türbinlerinde boşluk yapısı uygulamaları. In M. Makaracı (Ed.), *Makine Teknolojileri ve Taşıt Enerji Sektörleri İçin Malzeme ve Tasarım Metodları I* (BİDGE Yayınları, Vol. 1, Issue 1, pp. 19–43). Bidge Yayınları.

Tanürün, H. E. (2023c). H-Darrieus Dikey Eksenli Rüzgâr Türbinlerinde J-Tipi Kanat Yapısı Uygulamalar. In M. Makaracı (Ed.), *Makine Teknolojileri ve Taşıt Enerji Sektörleri İçin Malzeme ve Tasarım Metodları III* (BİDGE Yayınları, Vol. 1, pp. 83–102). Bidge Yayınları.

Tanürün, H. E. (2023d). Savonius dikey eksenli rüzgâr türbinlerinde deflektör yapisinin performans üzerine etkisinin kapsamli derlemesi . In C. Mavruk (Ed.), *5. Internatıonal Antalya*

Scıentıfic Research And Innovatıve Studıes Congress (pp. 235–245). IKSAD.

Tanürün, H. E. (2023e). Taguchi Yöntemiyle Sağlamlık Oranının Dikey Eksenli Rüzgâr Türbini Performansına Olan Etkisinin Sayısal Olarak İncelenmesi. *Journal of Materials and Mechatronics: A*, *4*(2), 355–372. https://doi.org/10.55546/JMM.1295748

Tanürün, H. E. (2024). Improvement of vertical axis wind turbine performance by using the optimized adaptive flap by the Taguchi method. *Energy Sources, Part A: Recovery, Utilization and Environmental Effects*, *46*(1), 71–90. https://doi.org/10.1080/15567036.2023.2279264

Tanürün, H. E. (2025a). Aerodynamic Performance Optimization of a Vertical-Axis Wind Turbine Using Blade–Spoke Connection and Pitch Angle via the Taguchi Method. *Bulletin of the Polish Academy of Sciences Technical Sciences*, 156796–156796. https://doi.org/10.24425/BPASTS.2025.156796

Tanürün, H. E. (2025b). Comprehensive review of the effect of flap technologies in H-Darrieus vertical axis wind turbines. *Pamukkale University Journal of Engineering Sciences*, *31*(4), 522–535. https://doi.org/10.5505/pajes.2024.09147

Tanürün, H. E. (2025c). Experimental investigation of an adverse curved slot flap on the aerodynamic performance of a NACA 63(4)-421 airfoil. In A. Sözen, N. Yücel, İ. Horuz, N. F. Özdil, & B. D. Mert (Eds.), *25th congress on thermal science and technology with international participation* (pp. 349–355).

Tanürün, H. E., & Acır, A. (2019). The Numeric Analysis of Tubercle Effect on Modified NACA-0015 Airfoil. *Journal of Polytechnic*, *22*(1), 185–195. https://doi.org/10.2339/POLITEKNIK.391800

Tanürün, H. E., & Acır, A. (2022). Investigation of the hydrogen production potential of the H-Darrieus turbines combined with various wind-lens. *International Journal of Hydrogen Energy*, *47*(55), 23118–23138. https://doi.org/10.1016/j.ijhydene.2022.04.196

Tanürün, H. E., Akın, A. G., & Acır, A. (2021). Numerical investigation of rib structure effects on performance of wind turbines. *Journal of Polytechnic*, *24*(3), 1219–1226. https://doi.org/10.2339/POLITEKNIK.845804

Tanürün, H. E., Akın, A. G., Acır, A., & Şahin, İ. (2024). Experimental and Numerical Investigation of Roughness Structure in Wind Turbine Airfoil at Low Reynolds Number. *International Journal of Thermodynamics*, *27*(3), 26–36. https://doi.org/10.5541/IJOT.1455513

Tanürün, H. E., Ata, İ., Canlı, M. E., & Acır, A. (2019). Farklı Açıklık Oranlarındaki NACA-0018 Rüzgâr Türbini Kanat Modeli Performansının Sayısal ve Deneysel İncelenmesi. *Journal of Polytechnic*, *0900*(2), 371–381. https://doi.org/10.2339/politeknik.500043

Tanürün, H. E., Yıldız, A., & Seyhan, M. (2026). Aerodynamic performance analysis of a NACA 63(4)-421 airfoil equipped with a trailing edge slot at suction side. *Experimental Thermal and Fluid Science*, *171*, 111604. https://doi.org/10.1016/J.EXPTHERMFLUSCI.2025.111604

Uma Reddy, K., Deb, B., & Roy, B. (2023). A numerical and experimental study on the performance of a conventional H-Darrieus wind rotor with auxiliary blades. *Ocean Engineering*, *280*, 114697. https://doi.org/10.1016/J.OCEANENG.2023.114697

Uma Reddy, K., Deb, B., Roy, B., & Majumder, P. (2024). Experimental and numerical analysis of NREL S823 airfoil with auxiliary airfoil integration. *Energy Sources, Part A: Recovery, Utilization and Environmental Effects*, *46*(1), 13633–13653. https://doi.org/10.1080/15567036.2024.240747

van Hooff, T., Blocken, B., Aanen, L., & Bronsema, B. (2011). A venturi-shaped roof for wind-induced natural ventilation of buildings: Wind tunnel and CFD evaluation of different design configurations. *Building and Environment*, *46*(9), 1797–1807. https://doi.org/10.1016/J.BUILDENV.2011.02.009

Wang, H., Zhang, B., Qiu, Q., & Xu, X. (2017). Flow control on the NREL S809 wind turbine airfoil using vortex generators. *Energy*, *118*, 1210–1221. https://doi.org/10.1016/J.ENERGY.2016.11.003

Wang, L., Alam, M. M., Rehman, S., & Zhou, Y. (2022). Effects of blowing and suction jets on the aerodynamic performance of wind turbine airfoil. *Renewable Energy*, *196*, 52–64. https://doi.org/10.1016/J.RENENE.2022.06.126

Wang, X., Ali, A., Ke, H., Huang, B., & Yang, J. (2025). Numerical simulation of aerodynamic performance degradation of NACA0012 airfoils under icing conditions for vertical-axis wind turbines. *Case Studies in Thermal Engineering*, *72*, 106433. https://doi.org/10.1016/J.CSITE.2025.106433

Wang, Y., Sun, X., Dong, X., Zhu, B., Huang, D., & Zheng, Z. (2016). Numerical investigation on aerodynamic performance of a novel vertical axis wind turbine with adaptive blades. *Energy Conversion and Management*, *108*, 275–286. https://doi.org/10.1016/J.ENCONMAN.2015.11.003

Wang, Z., & Zhuang, M. (2017). Leading-edge serrations for performance improvement on a vertical-axis wind turbine at low tip-speed-ratios. *Applied Energy*, *208*, 1184–1197. https://doi.org/10.1016/J.APENERGY.2017.09.034

Xu, J., Zhao, J., & Chang, J. (2025). Effect of Different Voltage Frequencies of Plasma Actuators on Wind Turbine Blade Lift and Rudder Efficiency. *Processes 2025, Vol. 13, Page 1032*, *13*(4), 1032. https://doi.org/10.3390/PR13041032

Xu, Z., Feng, Y. H., Zhao, C. Y., Huo, Y. L., Li, S., Hu, X. J., & Zhong, Y. J. (2018). Experimental and numerical investigation on aerodynamic performance of a novel disc-shaped wind rotor for the small-scale wind turbine. *Energy Conversion and Management*, *175*, 173–191. https://doi.org/10.1016/J.ENCONMAN.2018.09.003

Yildiz, A., Seyhan, M., & Tanürün, H. E. (2025). Experimental Investigation of a Passive Flexible Flag Control on an Adversely Slotted Airfoil. *8th International Conference on Applied Engineering and Natural Sciences*, 146–152.

Yıldız, A., Tanürün, H. E., Es, H. A., & Seyhan, M. (2025). Multi-response optimization of slotted airfoil for total aerodynamic performance: a Taguchi methodology with fuzzy decision support. *Aerospace Science and Technology*, 111408. https://doi.org/10.1016/J.AST.2025.111408

Yousefi Roshan, M., Khaleghinia, J., Eshagh Nimvari, M., & Salarian, H. (2021). Performance improvement of Darrieus wind turbine using different cavity layouts. *Energy Conversion and Management*, *246*. https://doi.org/10.1016/j.enconman.2021.114693

Zamani, M., Nazari, S., Moshizi, S. A., & Maghrebi, M. J. (2016). Three dimensional simulation of J-shaped Darrieus vertical axis wind turbine. *Energy*, *116*, 1243–1255. https://doi.org/10.1016/J.ENERGY.2016.10.031

Zavarian, Z., Abdizadeh, G. R., & Noori, S. (2023). Numerical investigation of the effect of dielectric barrier discharge plasma actuator-induced momentum jet parameters on flow control of an oscillating wind turbine airfoil. *Physics of Fluids*, *35*(6). https://doi.org/10.1063/5.0153485/2900216

Zhang, D., Wang, J., Lin, Y., Si, Y., Huang, C., Yang, J., Huang, B., & Li, W. (2017). Present situation and future prospect of renewable energy in China. *Renewable and Sustainable Energy Reviews*, *76*, 865–871. https://doi.org/10.1016/J.RSER.2017.03.023

Zhang, L., Gu, J., Hu, K., Zhu, H., Miao, J., Li, X., Ma, D., Mi, Y., & Wang, Z. (2021). Influences of trailing edge split flap on the aerodynamic performance of vertical axis wind turbine. *Energy Science and Engineering*, *9*(1), 101–115. https://doi.org/10.1002/ESE3.818

Zhu, C., Qiu, Y., Feng, Y., Wang, T., & Li, H. (2022). Combined effect of passive vortex generators and leading-edge roughness on dynamic stall of the wind turbine airfoil. *Energy Conversion and Management*, *251*. https://doi.org/10.1016/j.enconman.2021.115015

Zhu, H., Hao, W., Li, C., Luo, S., Liu, Q., & Gao, C. (2021). Effect of geometric parameters of Gurney flap on performance enhancement of straight-bladed vertical axis wind turbine. *Renewable Energy*, *165*, 464–480. https://doi.org/10.1016/j.renene.2020.11.027

DESIGN METHODOLOGIES AND PERFORMANCE ANALYSIS OF ENERGY SYSTEMS